Other Geologic Investigations

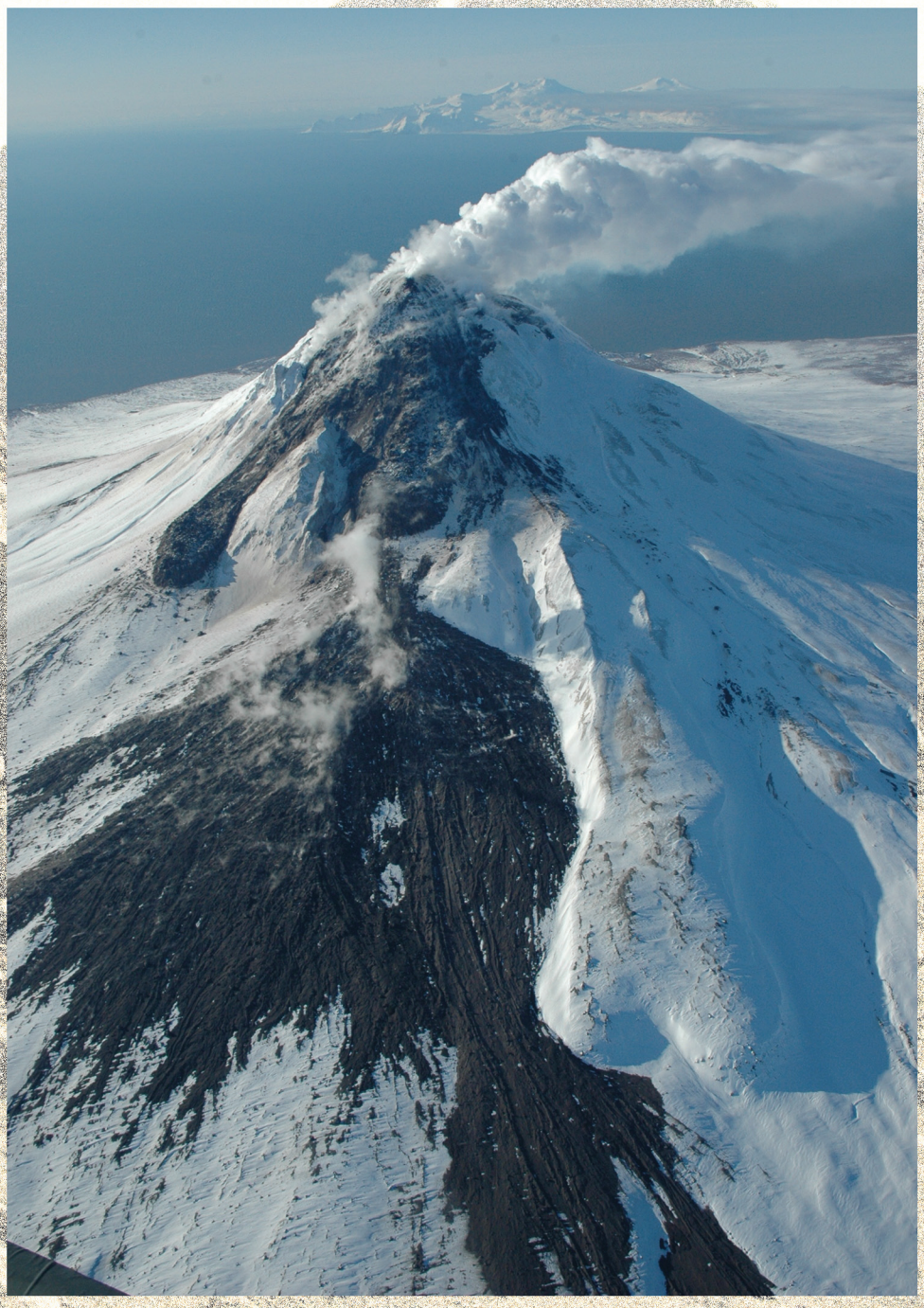

Oblique aerial view of the north side of Augustine Volcano on April 6, 2006, showing deposits from the 2006, eruption. A strong steam plume rises from the summit, and the northeast and north lava flows are visible on the upper parts of the edifice. Snow free area in foreground is hot pyroclastic deposits from the 2006 eruption. Alaska Volcano Observatory photo by R.G. McGimsey.

The 2006 Eruption of Augustine Volcano, Alaska
Power, J.A., Coombs, M.L., and Freymueller, J.T., editors
U.S. Geological Survey Professional Paper 1769

Chapter 13

Ejecta and Landslides from Augustine Volcano Before 2006

By Richard B. Waitt[1]

Abstract

A late Wisconsin volcano erupted onto the Jurassic-Cretaceous sedimentary bedrock of Augustine Island in lower Cook Inlet in Alaska. Olivine basalt interacting with water erupted explosively. Rhyolitic eruptive debris then swept down the south volcano flank while late Wisconsin glaciers from mountians on western mainland surrounded the island. Early to middle Holocene deposits probably erupted onto the island but are now largely buried. About 5,200, 3,750, 3,500, and 2,275 yr B.P. Augustine ash fell 70 to 110 km away.

Since about 2,300 yr B.P. several large eruptions deposited coarse-pumice fall beds on the volcano flanks; many smaller eruptions dropped sand and silt ash. The steep summit erupting viscous andesite domes has repeatedly collapsed into rocky avalanches that flowed into the sea. After a collapse, new domes rebuilt the summit. One to three avalanches shed east before about 2,100 yr B.P., two large ones swept east and southeast between about 2,100 and 1,700 yr B.P., and one shed east and east-northeast between 1,700 and 1,450 yr B.P. Others swept into the sea on the volcano's south, southwest, and north-northwest between about 1,450 and 1,100 yr B.P., and pyroclastic fans spread southeast and southwest. Pyroclastic flows and surges poured down the west and south flanks and a debris avalanche plowed into the western sea between about 1,000 and 750 yr B.P. A small debris avalanche shed south-southeast between about 750 and 390 yr B.P., and large lithic pyroclastic flows went southeast.

From about 390 to 200 yr B.P., three rocky avalanches swept down the west-northwest, north-northwest, and north flanks. The large West Island avalanche reached far beyond a former sea cliff and initiated a tsunami. Augustine's only conspicuous lava flow erupted on the north flank.

In October 1883 a debris avalanche plowed into the sea to form Burr Point on the north-northeast; then came ashfall, pyroclastic surge, and pyroclastic flows. Eruptions in 1935 and 1963–64 grew summit lava domes that shed coarse rubbly lithic pyroclastic flows down the southwest and south flanks. Eruptions in 1976 and 1986 grew domes that shed large pyroclastic flows northeast, north, and north-northwest.

The largest debris avalanches off Augustine sweep into the sea and radiate tsunami about lower Cook Inlet.

Introduction

Augustine's 2006 eruption embellished a mountain cone built by countless eruptions and mass-wastages over more than 15,000 years. This chapter summarizes pre-2006 surface geology detailed in a stratigraphic monograph and geologic map (Waitt and Begét, 2009). Like many other stratovolcanoes, Augustine has erupted repeatedly, sending pyroclastic flows down its flanks and depositing tephra near and far. Unusual about this cone is the rapidity with which domes build near the summit and then fail as debris avalanches. During the past two millennia or so Augustine has shed more than a dozen such rocky avalanches into the sea.

Setting and Rocks

Augustine Island, about 90 km^2, lies in southwestern Cook Inlet in southcentral Alaska (fig. 1*A*). Its nearly symmetrical mountain summit before 2006 peaked at 1,254 m (figs. 1*B*, 2). This island volcano lies along an active segment of the eastern Aleutian arc and 90–140 km above a seismic Benioff zone (Kienle and Swanson, 1983). The region's most explosive volcano, Augustine has erupted countless times since the end of the last ice age, including historical eruptions in 1812, 1883, 1935, 1963–64, 1976, 1986, and 2006.

Augustine's summit consists of many overlapping andesitic lava domes extruded intermittently over centuries. Most coastal cliffs expose diamicts comprising angular domerock cobbles and boulders, some as large as 4–12 m, all set in a

[1]U.S. Geological Survey, Cascades Volcano Observatory, 1300 SE Cardinal Court, Vancouver, WA 98683.

sandy matrix rich in very angular fragments. The surfaces of most diamicts are hummocky, many meters in relief. These deposits resemble the debris avalanche off Mount St. Helens in May 1980 (Voight and others, 1983; Glicken, 1998). That avalanche revealed the origin of hummocky, rocky diamicts at the bases of many other stratovolcanoes. Since the 1980s such landscape on Augustine's lower flanks has been interpreted as deposits of debris avalanches (Siebert and others, 1989, 1995; Begét and Kienle, 1992; Waitt and Begét, 1996, 2009).

Augustine's porphyritic andesite lava domes and flows range from dark gray to light gray to reddish (oxidized). Debris avalanches and lithic pyroclastic flows contain angular boulders and smaller fragments of this andesite. The ashy flows and coarse fall layers are rich in white to buff pumice. Rare inliers of fragmental olivine basalt lie on the volcano's south flank. Augustine rocks scatter chemically across the SiO_2 field of andesite (LeBas and Streckeisen, 1991), and glass-fraction analyses of prehistoric through 1996 pumice range from dacite to rhyolite. A few whole-rock analyses spill into the fields of basaltic andesite or low-silica dacite, but I call all these look-alikes andesite.

Augustine rocks have varied neither mineralogically nor chemically during the past few thousand years (Kienle and Swanson, 1985; Daley, 1986; Larsen and others, 2010). Each eruption seems to emit a similar suite of porphyritic andesite. For the 1976 eruption Johnston (1978) inferred that basalt

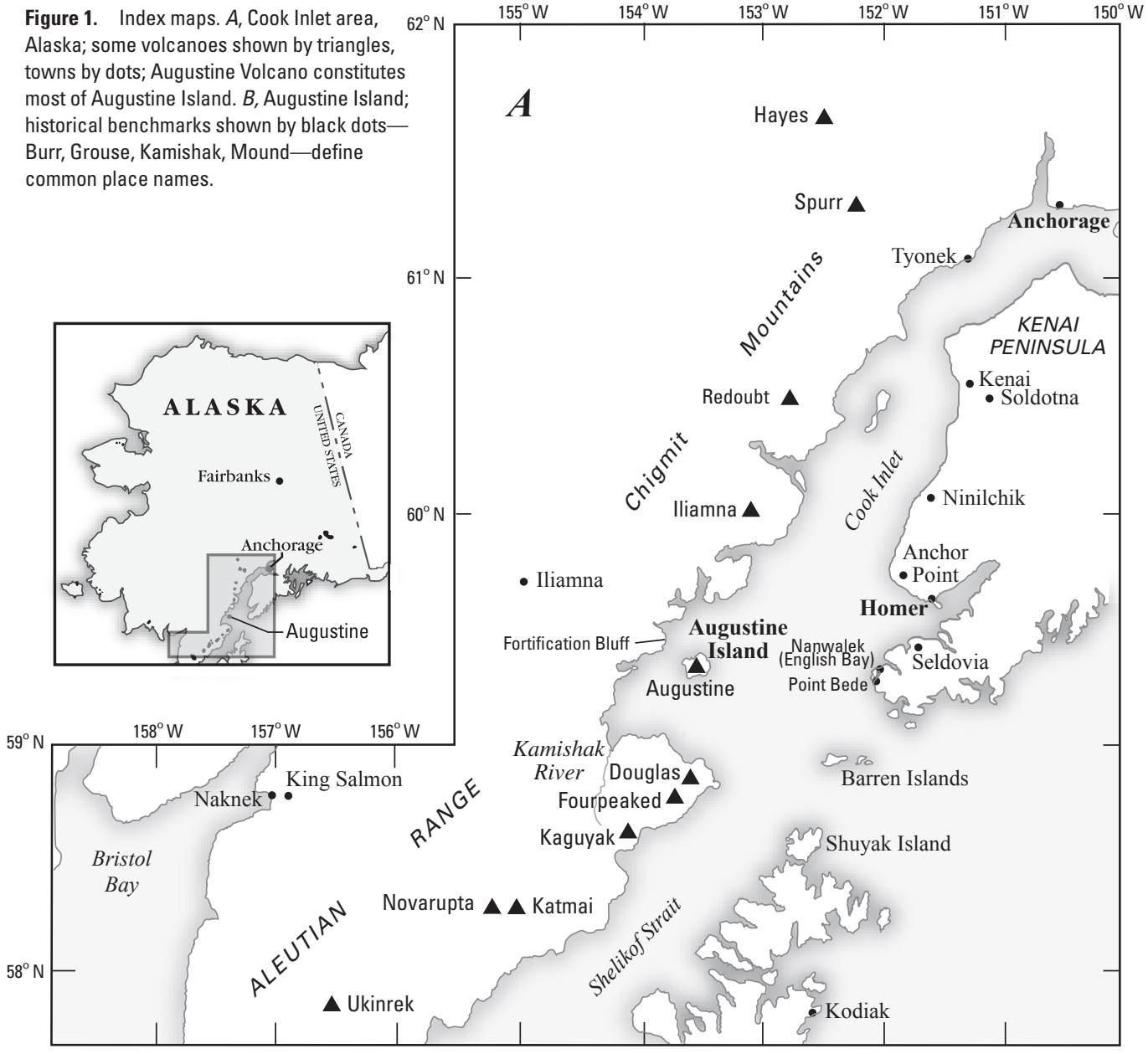

Figure 1. Index maps. *A*, Cook Inlet area, Alaska; some volcanoes shown by triangles, towns by dots; Augustine Volcano constitutes most of Augustine Island. *B*, Augustine Island; historical benchmarks shown by black dots—Burr, Grouse, Kamishak, Mound—define common place names.

magma intruded into a dacite chamber, the two partly mixing before erupting. Such magmas also mixed to trigger the 1986 and 2006 eruptions (Roman and others, 2006; Larsen and others, 2010). Variegated "mixed-magma" pumice also lies in the deposits of several prehistoric eruptions.

Chronology and Geomorphology

A few dozen radiocarbon dates from organic materials interbedded with tephra (fall deposits) on Augustine Island or at distal sites give limiting ages of the tephras (Waitt and Begét, 2009, table 2). Once bracketed by radiocarbon dates, a distinguishable tephra is a date by proxy.

Tephra blankets parts of Augustine's flanks and veneers mainland areas far downwind—eastward about 80 percent of the time. Stratigraphy on Augustine's east and southeast flanks shows six coarse pumiceous layers separated by layers of peat enclosing sand and silt ashes. In upward succession (fig. 3; table 1) the coarse tephras are G (2,100 yr B.P.), I (1,700 B.P.), H (1,500–1,400 B.P.), C (1,200–1,000 B.P.), M (750 B.P.), and B (390 yr B.P.). They are typically 10 to 80 cm thick along depositional axes and taper off laterally. The lower coarse tephras—G, I, H, and C—drifted east and southeast; tephra M drifted south and tephra B strongly northeast (Waitt and Begét, 2009, fig. 7). On Augustine's lower flanks large fragments in the coarse tephras are 1–5 cm in diameter. Between and atop these coarse tephras lie many sand-silt tephras of lesser eruptions including the seven historical ones from 1812 to 2006 (figs. 3, 4).

Table 1 includes the range of uncertainty in calendar ages if the raw radiocarbon dates were calibrated. Calibration does not much change discussion about the past 2,200 years, only adds a range of uncertainty. To keep text readable, dates remain in raw (uncalibrated) round numbers.

Geomorphic character suggests a deposit's origin and age. A deposit more vegetated than its otherwise identical neighbor must be older. Rocky debris fanning gently seaward must be much younger than its neighbor cut back to a high seacliff. A seacliff ceases to develop when a flow spreads beyond it and shifts the coast seaward. Seacliffs well back of Augustine's coasts tell of wave erosion arrested by new eruption deposits (fig. 5). Debris avalanches stand out from other

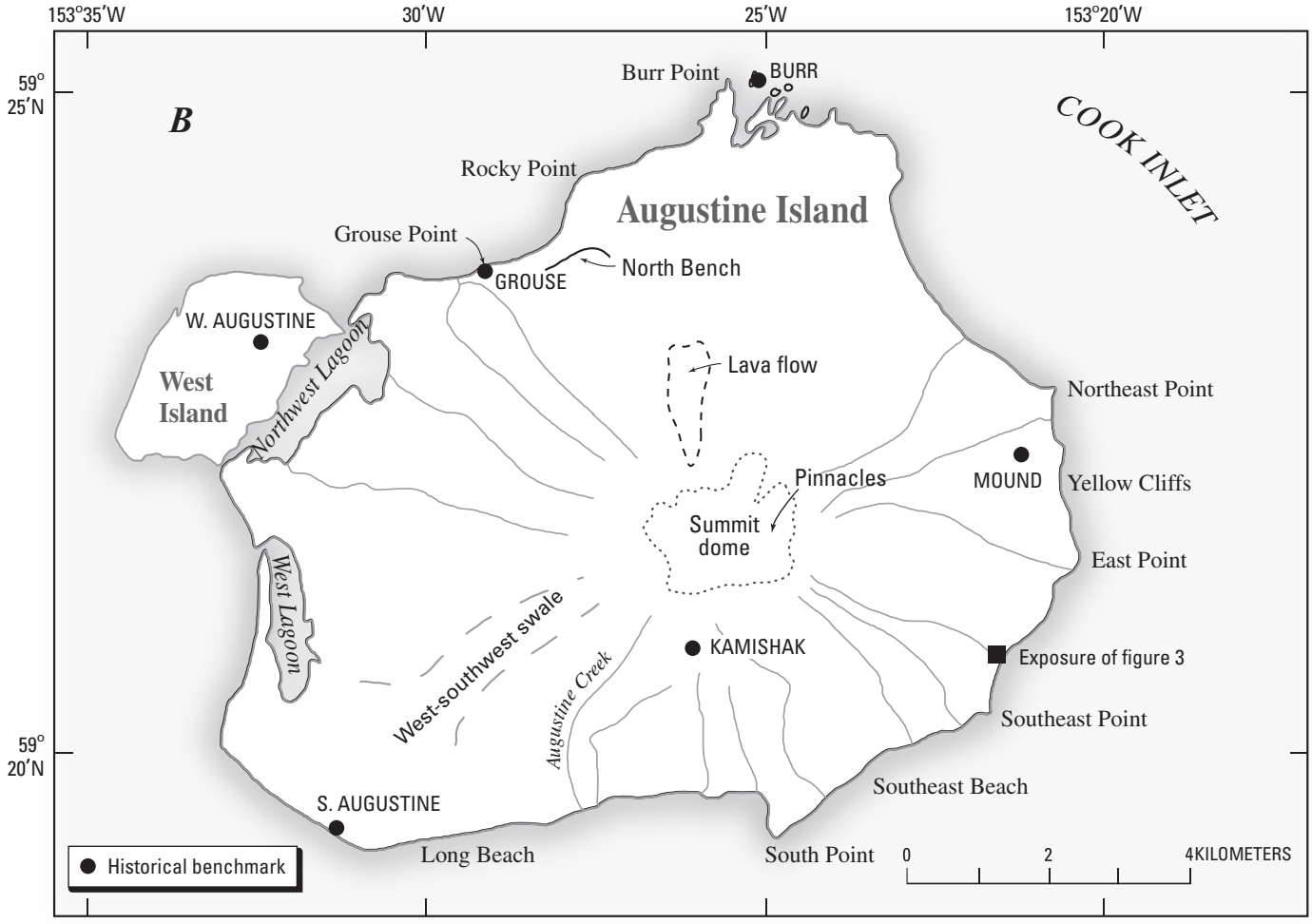

Figure 1.—Continued.

flow deposits by their huge angular dome-andesite boulders and topography of hummocks and depressions. Offshore of most of Augustine's avalanches, such hummocky topography also shows in bathymetric contours (fig. 6).

Mesozoic Rocks

Hard sedimentary bedrock reaching 400 m above the present south coast formed Augustine Island before the volcano existed (fig. 7). Fossils identify most of these hard layered rocks with the Upper Jurassic Naknek Formation (Detterman and Jones, 1974) on the western mainland (Detterman and Hartsock, 1966; Magoon and others, 1976). On Augustine Island the gently south-dipping Naknek comprises slope-forming siltstone to fine sandstone and cliff-forming sandstone. At higher altitudes, 350 to 400 m, friable sandstone and conglomerate contains *Inoceramus* and other fossils that correlate with the Upper Cretaceous Kaguyak Formation on mainland Cape Douglas to the south-southwest (Jones and Clark, 1973; Detterman and Jones, 1974). Cut by deep gullies, Mount Augustine's smooth and broad south slopes below 550 m are of this Jurassic-Cretaceous bedrock.

Pleistocene Deposits

A ridge 500 m long and 60 m high along the south coast consists of Naknek sandstone and overlying glacial deposits that crop out 200 m higher. Faults and open fissures riddle this coastal rock; bedding attitudes vary widely, their dips much steeper than in the upslope bedrock. This ridge is a Pleistocene block landslide that must have slid on seaward-dipping Naknek shale.

Diamicts containing striated pebbles to boulders of granite, diorite, gabbro, gneiss, greenstone, and chert crop out on the south flank. These unweathered exotic stones derive from the glaciated mountains along the west side of lower Cook Inlet probably during the late Wisconsin between 30,000 and 12,000 ^{14}C yr B.P. The stones as high as 290 m above sea level on Augustine, apparently the height to which glaciers spread across lower Cook Inlet during lowered sea levels

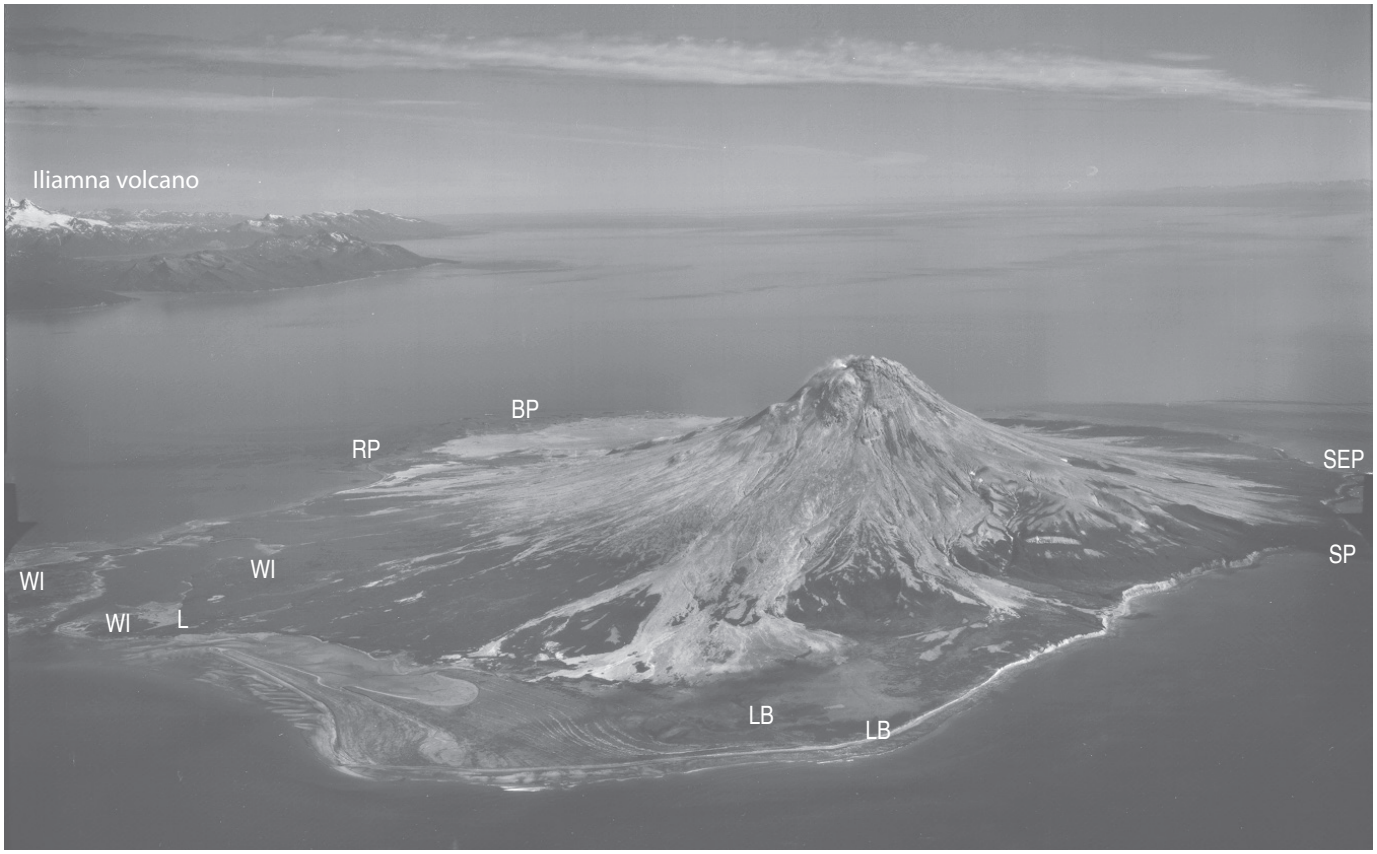

Figure 2. Oblique aerial view northeastward of Augustine Island and volcano. Much of vegetated (dark-toned) area of lower flanks is debris avalanches: BP, Burr Point; RP, Rocky Point; WI, West Island; L, Lagoon; SP, South Point; LB, Long Beach; SEP, Southeast Point. Light-toned areas are deposits of pyroclastic flows of 1963–64, 1976, and 1986 eruptions. The near point is built up over the last thousand years by seaward-accreting beach ridges capped by eolian sand. USGS photograph by Austin Post, August 25, 1987.

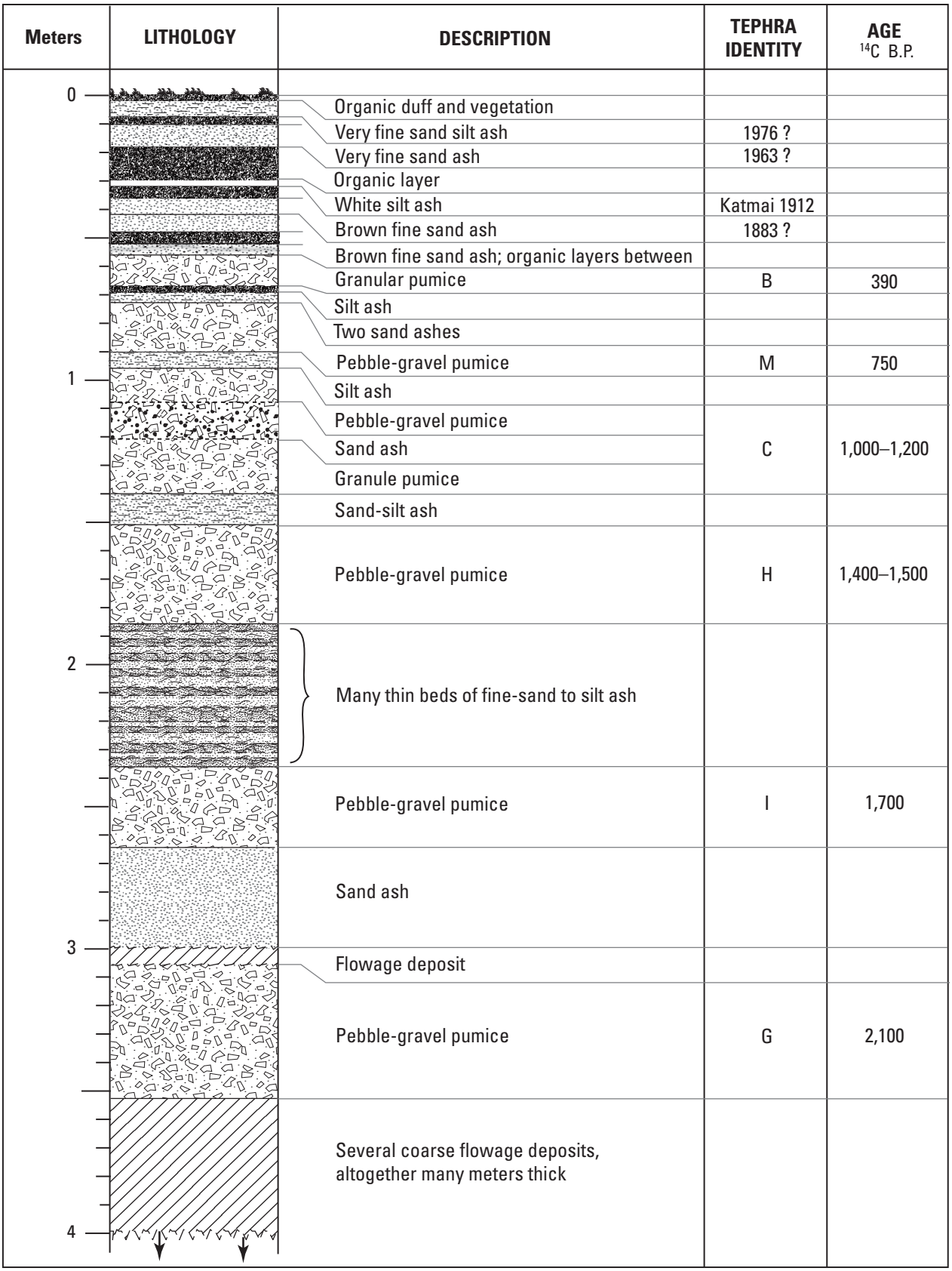

Figure 3. Tephra stratigraphy overlying flowage deposits on Augustine Island north of Southeast Point (fig. 2*B*). Flowage deposits below tephra G are each several meters thick. Radiocarbon ages are uncalibrated.

Table 1. Stratigraphy of coarse pumiceous "marker-bed" tephra layers and debris-avalanche deposits, Augustine Volcano.

Debris Avalanche	Tephra Layer	Approximate Age (^{14}C yr BP), or [AD]	Calibrated Age Range BP at 2σ confidence, or [AD]
Burr Point		[1883]	[1883]
Rocky Point			
West Island (incl. Grouse Pt.)			
• • • • • • • • •	B	390	310–510
Southeast Beach			
• • • • • • • • •	M	750	660–780
Lagoon			
• • • • • • • • •	C	1,000–1,200	750–1,300
Long Beach			
South Point			
North Bench (may be older)			
• • • • • • • • •	H	1,400–1,500	1,240–1,530
Northeast Point			
• • • • • • • • •	I	1,700	1,530–1,700
Southeast Point			
Yellow Cliffs			
• • • • • • • • •	G	2,100	1,990–2,150
East Point (perhaps comprises 3 separate avalanches)			

about 15,000 years ago (Hamilton and Thorson, 1983) and surrounded Augustine Island's mountain.

Augustine's south flank (fig. 7) exposes fragmental porphyritic olivine basalt and basaltic andesite, some beds cemented palagonite. Angular fragments scatter through low-angle cross beds containing 3- to 8-mm mud balls, and angular bombs have sagged 25 cm. Apparently these were water-propelled explosions, the beds emplaced wet. The upper 20 cm of this basaltic hyaloclastite is interlayered with the base of overlying rhyolitic tephra. So olivine basalt erupted from a south-flank vent while pumice erupted upslope, likely the summit.

Holocene Tephra, Flows, and Lava Domes

Sections high on Augustine's south side expose bedded deposits of pumiceous falls, lithic falls, and pumiceous pyroclastic flows. A peat layer halfway up one tall section dates to 2,160 yr B.P. Except on such inliers, deposits of early and middle Holocene eruptions on Augustine Island lie buried beneath younger eruptive debris. But on Shuyak Island 110 km southeast of Augustine (fig. 1*A*), two tephras chemically fingerprinted to Augustine date between 6,460 and 5,020 yr B.P., where a higher Augustine tephra dates to 3,620–3,360 yr B.P. (Waitt and Begét, 2009, plate 2). At Kamishak Creek 70 km southwest of Augustine Island, an Augustine-chemistry fall tephra dates between 3,850 and 3,660 yr B.P. (Riehle and others, 1998, fig. 8). A likely Augustine ash near Homer 110 km northeast of Augustine dates to about 2,275 yr B.P. Early to middle Holocene Augustine tephras lie on Fortification Bluff west-northwest of Augustine (Riehle and others, 1998; Waitt and Begét, 2009).

Gray porphyritic andesite forms Kamishak dome at altitude 513 m on Augustine's south flank (figs. 2, 7). Porphyritic andesite also forms domes F and P, knobs at 1,025 and 910 m on the upper northwest flank. West Island debris avalanche

must have left a theater-shaped scar in this area, so domes F and P postdate about 370 yr B.P. but precede historical eruptions. Several overlapping prehistoric domes form the east and south sides of the summit cone. Several historical domes overlap this old dome rock. All-but-buried porphyritic andesite crops out here and there far below these domes, far enough down to be lava flows.

Prehistoric Late Holocene Deposits

Most of Augustine's lower-flank deposits are bouldery diamicts, each an unsorted mixture of angular clasts of summit-dome rock of all sizes, sand to enormous boulders. Most of them I infer as debris avalanches but a few as lithic pyroclastic flows. This summary piece skips soon from description (diamict) to interpretion (debris avalanche).

Between about 2,500 and 1,450 ^{14}C yr B.P.

A continuous high sea cliff between Southeast Point and Northeast Point exposes bouldery debris and intervening tephra that divide into at least four thick diamicts, probably debris avalanches.

East Point Debris Avalanches

The lowest of these four, East Point diamict beneath tephra G (table 1), forms the lower 13 m of this seacliff. Its angular andesite boulders as large as 5–7 m are set in a sand-gravel diamictic matrix of shattered andesite. A few prismatically jointed clasts must have been hot juvenile dome rocks. Fluvial deposits within the diamict section suggest it comprises two or three successive avalanches.

Yellow Cliffs Debris Avalanche

Overlying East Point debris avalanches and tephra G, a yellowish diamict 5–9 m thick forms the middle to upper part of the east-coast seacliff. Matrix and clasts as large as 3.5 m are strongly altered and soft, yet the deposit contains sporadic huge pods of scarcely altered andesite diamict. These unoxidized zones and this diamict's position sandwiched between unoxidized diamicts show that the alteration had occurred in the summit source area before landsliding.

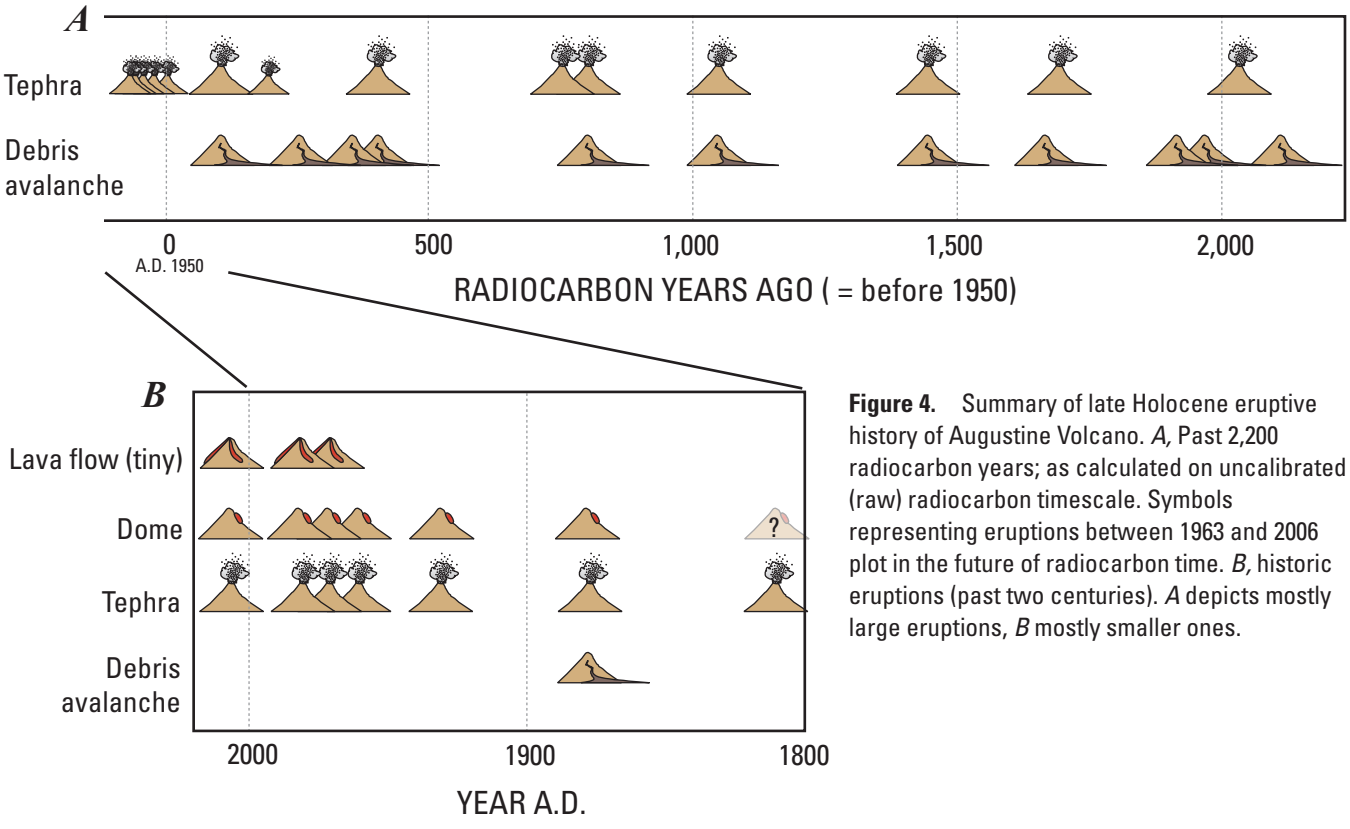

Figure 4. Summary of late Holocene eruptive history of Augustine Volcano. *A,* Past 2,200 radiocarbon years; as calculated on uncalibrated (raw) radiocarbon timescale. Symbols representing eruptions between 1963 and 2006 plot in the future of radiocarbon time. *B,* historic eruptions (past two centuries). *A* depicts mostly large eruptions, *B* mostly smaller ones.

Southeast Point and Northeast Point Debris Avalanches

Overlying Yellow Cliffs avalanche in the coastal cliff near Southeast Point, a diamict at least 8 m thick contains boulders as large as 4–7 m (fig. 8) and a scarcely altered matrix. This Southeast Point avalanche extends to Northeast Point where tephra I overlies it, overlain in turn by Northeast Point diamict (fig. 9).

Along the top of the east-coast cliff between tephras I and H, a coarse diamict at Northeast Point is as thick as 20 m, contains angular andesite boulders as large as 7 m (fig. 8), and traces up gullies to the base of the summit domes. Beneath mantling tephra and peat, the surface's sharp local relief is at least 6 m. By these properties it is clearly another rocky avalanche. In spots the diamict is strikingly monolithologic, every fragment very angular. A dome block 30 m long is more disaggregated than "jig-saw" blocks in the 1980 Mount St. Helens avalanche (Glicken, 1996). So immense a block could only have piggybacked atop an avalanche.

At Northeast Point the deposit crosses a coastwise scarp 650 m long and 30 m high (fig. 5), a seacliff cut back into the Yellow Cliffs and older avalanches. Northeast Point avalanche overrode and largely buried this scarp. Boulders as large as 5 m extend 600 m offshore. From there the sea has eroded this avalanche back to its present seacliff.

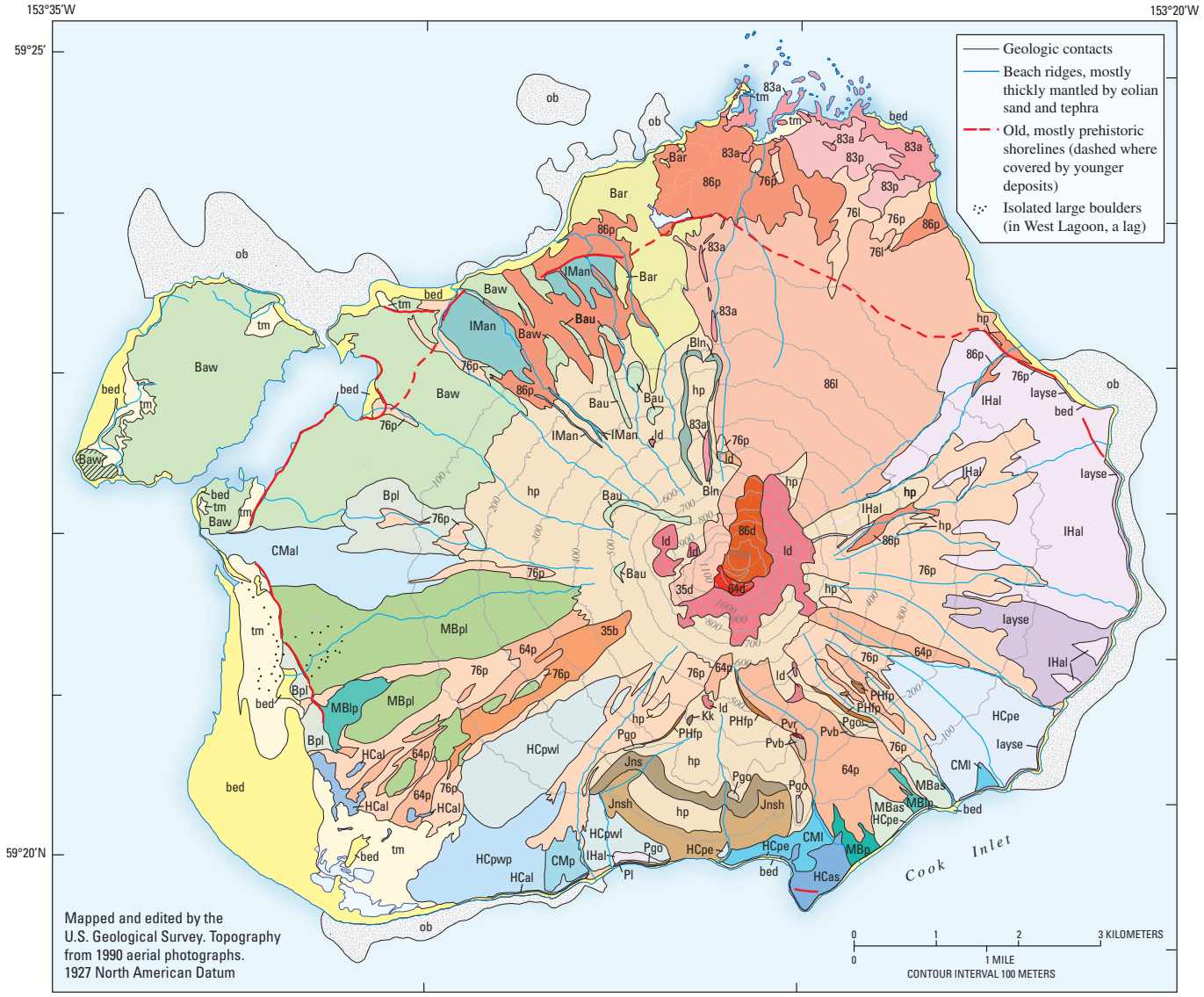

Figure 5. Pre-2006 geologic map of Augustine Island greatly simplified from Waitt and Begét (2009, plate 1). Ruled area of West Island is planed-off hummocks.

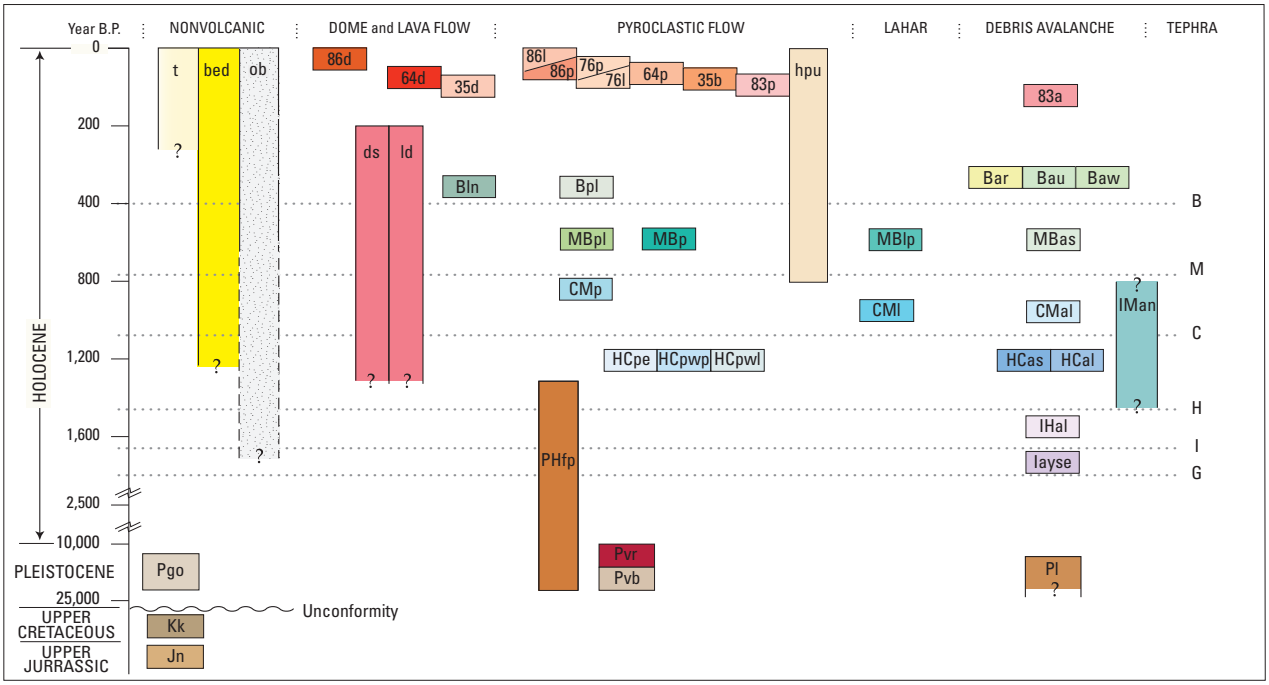

RECENT TO PREHISTORIC

tm Tidal and marsh alluvium.

bed **Beach and eolian deposits**—Loose medium to coarse sand in bodies parallel to coast.

ob Offshore boulders

HISTORICAL ERUPTIONS

86dg 1986 lava dome and agglutinate—Porphyritic andesite.

86l / 86p 1986 lithic and pumiceous pyroclastic flow.

76l / 76p 1976 lithic and pumicous pyroclastic flow.

64d 1963-64 Lava dome—Porphyritic andesite.

64p 1963-64 pyroclastic flow and lahar.

35d 1935 lava dome—Porphyritic andesite.

35b 1935 blocky rubble—Shed from summit dome.

83p 1883 pyroclastic flow and surge.

83a 1883 debris avalanche—Bouldery diamict.

hp Pyroclastic flow, lahar, and fall deposits of historic and prehistoric eruptions.

PREHISTORIC

Younger than about 390 ^{14}C yr B.P.

Bln North Slope lava flow—Massive porphyritic andesite.

Bar Rocky Point debris avalanche—Bouldery nonsorted diamict.

Bpl Lithic pyroclastic flow (or lahar?).

Bau Undifferentiated small debris avalanches.

Baw **West Island debris avalanche**—Bouldery diamict.

Between about 750 and 390 ^{14}C yr B.P.

Lithic pyroclastic-flow or lahar(?):

MBpl Bouldery diamict of andesite, finely lobate and leveed.

MBp Pyroclastic flow.

MBas Southeast Beach debris avalanche—Bouldery diamict.

MBlp Lahar or pyroclastic flow

Between about 1,100 and 750 ^{14}C yr B.P.

CMal Lagoon debris avalanche—Bouldery diamict.

CMp Pyroclastic flow.

CMl Lithic pyroclastic flow (or lahar)—Cobble gravel to gravelly sand.

Between about 1,450 and 1,100 ^{14}C yr B.P.

lMan North Bench debris avalanche—Bouldery diamict.

HCpe **Southeast pyroclastic fan**—Boulders to gravelly sand.

Southwest pyroclastic fan:

HCpwp Pumiceous pyroclastic flow—Pumiceous gravelly sand.

HCpwl Lithic pyroclastic flow—Cobble to boulder gravel.

HCas South Point debris avalanche—Bouldery diamict of angular andesite fragments.

HCal Long Beach debris avalanche—Bouldery diamict of angular fragments.

Between about 1,700 and 1,450 ^{14}C yr B.P.

lHal Northeast Point debris avalanche and lahar—Bouldery diamict of andesite fragments and sandy gravel.

Between about 2,500 and 1,800 ^{14}C yr B.P.

layse Yellow Cliffs, Southeast Point, and East Point debris avalanches—Bouldery diamicts of angular andesite fragments.

Lava domes (late(?) Holocene)

ds Pre-1883 summit-dome complex—Porphyritic-andesite domes forming east crater rim and upper east and south flanks.

ld Lava domes and flows —Inliers of porphyritic andesite. Includes Dome P on the northwest flank at altitude 910 m, Dome F on the northwest flank at altitude 1,025 m, Dome Kamishak on the south flank at altitude 513 m, and flatter inliers at levels 380–530 m on south and north flanks.

LATE PLEISTOCENE (TO HOLOCENE ?)

PHfp Fall and pyroclastic flows—Interbedded pumiceous and lithic pyroclastic flows and pumiceous falls.

LATE(?) PLEISTOCENE

Pgo Glacial deposits—Gravel veneer of diverse angular clasts of exotic diorite, granite, gneiss, gabbro, greenstone, limestone.

Pvr Rhyolitic pumiceous beds.

Pvb Basaltic hyaloclastite.

Pl Block landslide—Sandstone and shale of Naknek Formation highly jointed and faulted, riddled with open fissures, apparently a displaced block derived upslope from unit Jn.

PREDATING AUGUSTINE VOLCANO

Kk Kaguyak Formation (Upper Cretaceous)—Greenish fossiliferous sandstone and sandy pebble conglomerate.

Jn **Naknek Formation (Upper Jurassic)**—Cliff-forming sandstone overlying siltstone with thin sandstone interbeds.

Between about 1,450 and 1,100 ^{14}C yr B.P.

Several bodies of coarse bouldery diamict lie along Augustine's lower southwest, south, and southeast slopes, capped by tephra C but not by H.

South Point and Long Beach Debris Avalanches

Jutting 600 m seaward from the south coast, South Point diamict is at least 30 m thick. Its hummocky surface 10 m in relief includes angular porphyritic-andesite clasts as large as 9 m—properties showing it's a debris avalanche. South Point being broader and reaching more seaward than Northeast Point suggests its relative youth. The capping tephra-and-peat sequence 1–2 m thick has the C tephra near its base, stratigraphically proving relative youth. Yet eroded back into a high cliff, this coarse avalanche is geomorphically older than the weakly cliffed avalanches around the west and north coasts.

Long Beach diamict sparsely exposed on the lower southwest flank forms a belt of hummocks beyond 1976 ash-flows. Hummocks as much as 9 m high and 20 across—one mostly a 9-m boulder (fig. 10)—reveal the deposit as another coarse debris avalanche. Hummocks typically contain boulders as large as 6 m and are capped by tephra C. At low tide a large-boulder lag reaches half a kilometer off the south-southwest shore, and convoluted bathymetric contours reach farther (figs. 5, 6).

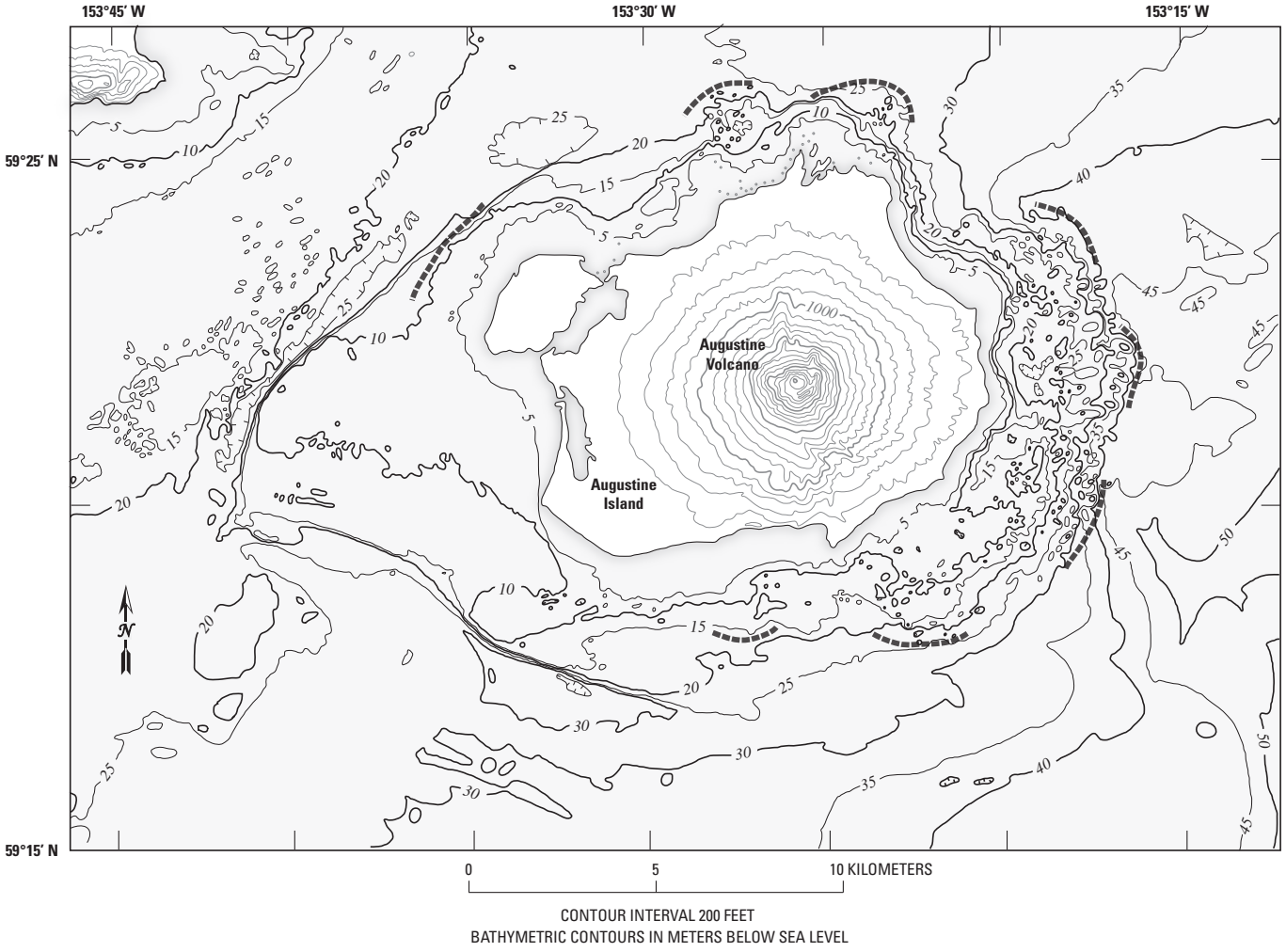

Figure 6. Conspicuously bumpy submarine topography revealing offshore distribution of debris avalanches. Heavy dashed line indicates approximate outer limits. The 200-ft (about 60 m) contours on Augustine Island and the 5-m contours of bathymetry are from U.S. Geological Survey 1:250,000 Iliamna quadrangle. Hummocky topography attributed to Augustine's debris avalanches extends to depth of 45 m and as far as 3.8 km off east coast and to depth of 25 m as far as 2.8 km off north coast. Farther areas of lumpy topography, such as 5–10 km west and northwest of West Island are from late Wisconsin glaciation or other nonvolcanic processes.

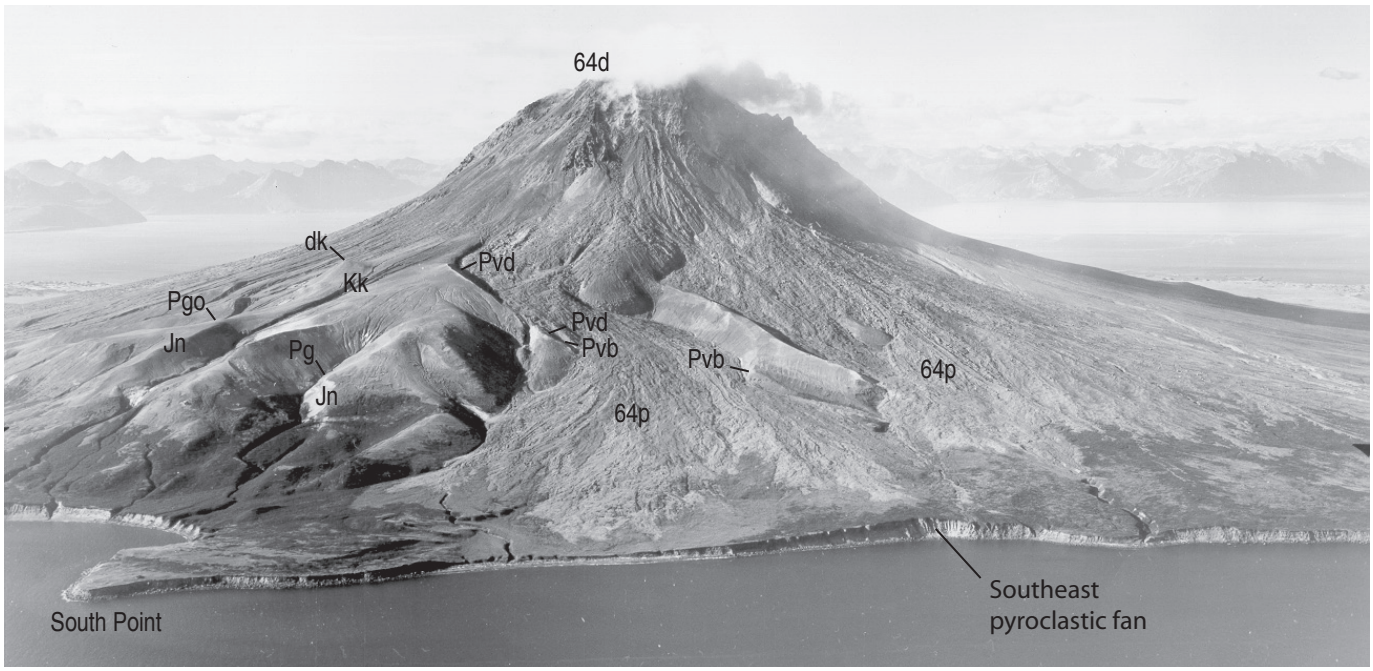

Figure 7. Oblique aerial view north-northwestward of Augustine Volcano. Most smooth, maturely dissected topography of south flank is Jurassic and Cretaceous bedrock (Jn, Kk) being gradually buried by Augustine's young cone and fall tephras. Shown are locations of Kamishak dome (dk) and Pleistocene deposits: basaltic hyaloclastite (Pvb), dacitic fall and flow deposits (Pvd), and glacial deposit (Pgo). Below 1964 dome (64d) are extensive coarse 1963–64 pyroclastic flows (64p). USGS photograph by Austin Post, September 3,1966.

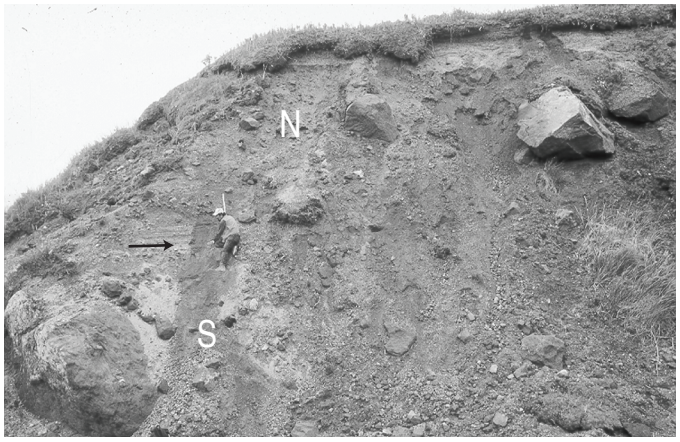

Figure 8. Bouldery Southeast Point debris avalanche (S) overlain by tephra I (small arrow at man), overlain in turn by bouldery Northeast Point debris avalanche (N), capped by tephra H and younger tephras and soils. East coast of Augustine Island.

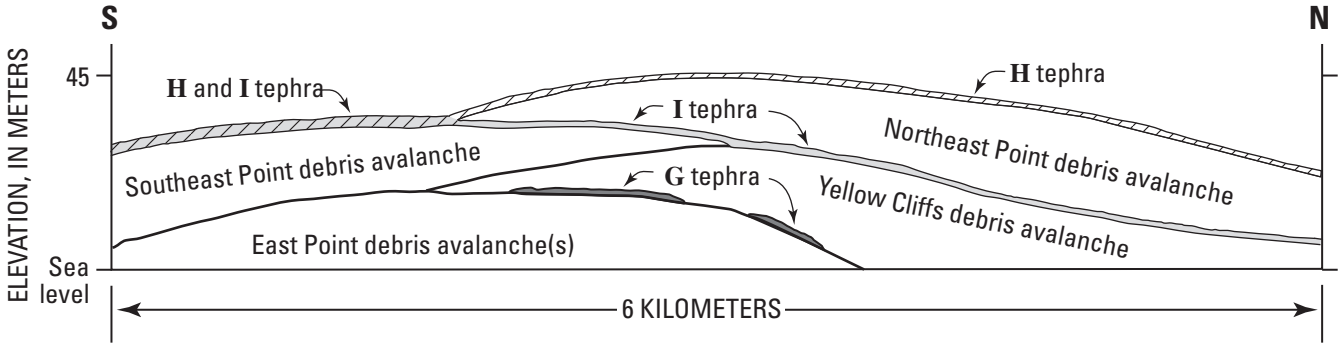

Figure 9. Schematic sketch of coastal cliffs along east side of Augustine Island showing stratigraphic relations of the four oldest debris avalanches and the three oldest coarse pumiceous-tephra marker beds: G, I, and H.

Southwest and Southeast Pyroclastic Fans

A steep angular-gravel fan on Augustine's southwest flank includes 6-m andesite boulders and is capped by tephra C. Many closely spaced levees and intricately lobate margins embellish its surface. These and other characteristics—it lacks hummocks—show it to be of lithic pyroclastic flows. In coastal cliffs a sandy pumiceous pyroclastic flow as thick as 16 m overlies the Long Beach avalanche. Pumice clasts concentrate in the oxidized upper 3 m, lithic clasts in the lower 10. One site reveals two such massive deposits—the lower 13 m thick and punctuated by openwork gas-escape pipes, the upper 4 m thick. Both flows followed the valley of Augustine Creek.

Pumiceous to lithic pyroclastic flows lie in the lower parts of the seacliff along Augustine's south-southeast coast. Numerous 6–9-m angular andesite boulders stud the surface upslope. Several closely paired levees trend downslope, curving into multilobate convex-downslope end ridges. Low in local relief, this deposit has the morphology of pyroclastic flow. The short distance (3 km) and steep slope (24°) from summit dome to deposit account for the huge blocks. It is roughly coeval with a lithic unit of southwest fan.

North Bench Debris Avalanche

At least 15 m thick, North Bench diamict comprises angular boulders as large as 5 m and its mildly hummocky topography has sparse local relief of 6 m. It is almost certainly another rocky avalanche. Pyroclastic flows and maybe tsunami overwash filled its lows and subdued its surface. A gently convex-seaward 23-m seacliff, the highest along Augustine's northwest coast, truncates the deposit. Younger deposits that descended intervening gullies and fanned along the coast isolated this cliff 400 m from the sea (fig. 5). North Bench avalanche is geomorphically much older than other northside avalanches.

Only the younger two coarse tephras lie on Augustine's northwest flank. In upslope gullies the avalanche is overlain by tephra B and younger ashes. Atop North Bench's seacliff, overlying strata are thin and only 1 or 2 ashes lie beneath the Katmai 1912 ash.

Figure 10. Nine-meter megaclast of summit-dome porphyritic andesite forming a single hummock of Long Beach debris-avalanche deposit on lower southwest flank of Augustine Volcano.

Between about 1,100 and 390 ^{14}C yr B.P.

Lagoon Debris Avalanche

Lagoon avalanche's sharp, hummocky local relief reaches 10 m and displays angular 3-m andesite boulders. Peat containing tephras M and B cap the highest coastal exposures and high hummocks inland. This avalanche apparently buried and rode beyond an older seacliff, perhaps the one truncating North Bench. Reaching 700 m seaward of this old cliff, Lagoon avalanche is only moderately cut back. Thus geomorphically it is fairly young. Hummocks below altitude 8 m along the coastal cliff are devoid of the M and B tephras. Water seems to have washed over these lower hummocks, stripping the tephras.

Pyroclastic Flow and Southeast Beach Avalanche

Atop a seacliff now isolated from the sea along the inner margin of West Lagoon is a 4-m bed of massive cobbly sand, apparently lithic pyroclastic flow, sandwiched between tephras B and M. This deposit formerly extended at least 300 m seaward, its legacy a lag of boulders as large as 2.5 m in West Lagoon. Waves must have eroded the deposit back, then to the west the long sand spit grew north, enclosing the lagoon. This low-relief deposit is marked upslope by intricately lobate termini and numerous levees containing large boulders, some with smaller stones piled behind. The levees and many small flow lobes reveal it as a lithic pyroclastic flow.

A bouldery diamict exposed in the upper part of the bluff along Southeast beach is studded with angular blocks as large as 2.5 m; lag boulders on the beach and in the surf zone reach 7 m. This small debris avalanche is sandwiched between tephras M and B.

Younger than about 390 ^{14}C yr B.P.

West Island Debris Avalanche

Separated from the northwest coast of Augustine Island by Northwest Lagoon (figs. 2, 5), West Island comprises a core of conical hummocks as high as 30 m (fig. 11*A*) covered in alder and scrub spruce, surrounded by lower hummocks,

some cut by seacliffs. Angular andesite boulders on West Island reach 5 m and lie in brecciated matrix. A boulder field visibly reaches at least 1¼ km offshore, submarine hummocky topography twice that (fig. 6). West Island avalanche mantles the volcano's lower northwest flank with angular boulders as large as 4 m. But most of it swept as much as 5 km beyond a sea cliff cut 8 to 18 m high that had been Augustine's coast (fig. 5). Up from the coast, tephra M (or B?) underlies the avalanche. Hummocks and lows on West Island are overlain by peat containing five sand ashes, three beneath Katmai 1912 ash—but no tephra B. The avalanche dates to about 370 yr B.P. (table 1).

A hummocky diamict about Grouse Point consists of angular boulders that on the wave-winnowed beach reach 7 m. One hummock 12 m in diameter seems to be largely one block of shattered andesite. Boulders extend nearly a kilometer seaward, and bathymetric contours show it extends offshore another half kilometer. Grouse Point diamict is considerably younger than North Bench avalanche—whose truncating seacliff it crosses—and seems instead an arm of West Island avalanche.

Loose gravelly sand 10–30 cm thick and containing angular juvenile andesite overlies West Island diamict at several sites. It resembles the deposit of the May 1980 pyroclastic surge at Mount St. Helens (Waitt, 1981). Apparently the large West Island landslide unleashed a similar but smaller surge (Siebert and others, 1989; Waitt and Begét, 2009).

Some nearshore southwestern hummocks of West Island are beveled off, capped by openwork boulders, and incised by steep-sided channels (fig. 11*B*). Apparently water rushed over them as the avalanche plowed into the sea. Atop one such hummock three sand ashes underlie the 1912 Katmai ash: the hydraulic planing occurred with the West Island avalanche, not later.

Just south of West Island avalanche, low parts of Lagoon avalanche are also devoid of tephras M and B, areas oddly strewn by large boulders. West Island avalanche's crash into the sea evidently raised a water wave that swept over seaward parts of Lagoon avalanche. These waves may have washed over North Bench, causing the meager stratigraphy atop a deposit geomorphically old by its high, straight seacliff.

Rocky Point Debris Avalanche

A coarse diamict about Rocky Point (fig. 12) contains angular 5-m andesite boulders and sharp, hummocky topography as high as 15 m. At low tide this debris forms bouldery wave-beveled islands and shoals to 12 km offshore. Rocky Point bristles with scrub alder but not the dense spruce of West Island and seems younger. Capping the coarse diamict is a weakly oxidized soil and organic layer, an 1883(?) sand ash, and the white-silt 1912 Katmai ash. The lone ash layer beneath the Katmai ash also shows this deposit younger than West Island.

North Slope Lava Flow

A lava flow of porphyritic andesite or basaltic andesite on Augustine's middle north flank (figs. 5, 13) issued from below the base of the summit-dome complex and terminates 450 m lower. About 100 m thick, it is the only conspicuous lava flow on the island. It seems not covered by Rocky Point avalanche, but the west levee of the 1883 Burr Point avalanche overlies and postdates the lava flow. This stratigraphy and the flow's azimuth suggest it came late in the eruption that began with Rocky Point avalanche.

Beach and Eolian Deposits

Southwest Augustine Island comprises dozens of subparallel accreted beach ridges and overlying eolian deposits (figs. 2, 5). Landward ridges underlie tephra M, 70 cm of eolian sand, and Katmai 1912 ash. Seaward ridges underlie thinner eolian sand atop pebbly beach gravel. This wide platform reflects the delivery of voluminus sand to the south coast before tephra M—the thick deposits of southwest and southeast pyroclastic fans, which longshore currents then moved west. At the back of sandy beaches round the island lie coastwise ridges of eolian sand, some more than a kilometer long. They accumulated over centuries, shown by interbeds of peat and sand ash, the Katmai 1912 ash near the top.

Historical Deposits

Capt. James Cook named "Mount St. Augustine" in 1778: "This Mountain is . . . conical . . . and of a very considerable height" (Beaglehole, 1967). English, French, Spanish, and Russian commercial voyages preceded George Vancouver's 1794 coastal mapping including Augustine: "a lofty, uniform, conical mountain" (Lamb, 1984). The many early accounts mention an Augustine eruption only in 1812, when Chernobory (Mount Augustine) "burned" and mainland villagers couldn't reach the island (Doroshin, 1870). This cryptically suggests pumiceous flows swept into the sea. Doroshin's sketch (fig 13*A*) shows a fresh-looking northside subsummit dome.

1883 Eruption

Augustine's 1883 eruption is partly documented by contemporaneous accounts. On the 6th of October 1883, Mount Augustine (Chernoburoy) generated ash plumes and a tsunami experienced at English Bay 85 km east. The record book of the Alaska Commercial Company [ACC] (1883) at English Bay that day includes:

Figure 11. Views of West Island debris-avalanche hummocks at Augustine Island, Alaska. *A,* View southeastward of southwest side of central core of high conical hummocks of West Island avalanche. *B*, Near oblique-aerial view west of oddly planed-off hummocks on southwest part of West Island. I infer the modified hummocks and scabland-like channels between them to have been eroded by a water wave across this part of the West Island debris avalanche—a tsunami being born.

Simkin, T., and Siebert, L., 1994, Volcanoes of the world (2d ed.): Tucson, Ariz., Geoscience Press, 349 p.

Vallance, J.W., Schilling, S.P., Devoli, G., Reid, M.E., Howell, M.M., and Brien, D.L., 2004, Lahar hazards at Casita and San Cristóbal Volcanoes, Nicaragua: U.S. Geological Survey Open-File Report 2001-468, 18 p., 3 map plates.

Voight, B., and Elsworth, D., 1997, Failure of volcano slopes: Geotechnique, v. 47, no. 1, p. 1–31.

Voight, B., Janda, R.J., Glicken, H., and Douglass, P.M., 1983, Nature and mechanics of the Mount St. Helens rockslide-avalanche of 18 May 1980: Geotechnique, v. 33, p. 243–273.

Waitt, R.B., 2010, Ejecta and landslides from Augustine Volcano before 2006, *in* Power, J.A., Coombs, M.L., and Freymueller, J.T., eds., The 2006 eruption of Augustine Volcano, Alaska: U.S. Geological Survey Professional Paper 1769 (this volume).

Waitt, R.B., and Begét, J.E., 2009, Volcanic processes and geology of Augustine Volcano, Alaska: U.S. Geological Survey Professional Paper 1762, 78 p., 2 map plates, [http://pubs.usgs.gov/pp/1762].

Waitt, R.B., Begét, J.E., and Kienle, J., 1996, Provisional geologic map of Augustine Volcano, Alaska: U.S. Geological Survey Open-File Report 96-516, 44 p., 1 map plate.

Watters, R.J., Zimbelman, D.R., Bowman, S.D., and Crowley, J.K., 2000, Rock mass strength assessment and significance to edifice stability, Mount Rainier and Mount Hood, Cascade Range Volcanoes: Pure and Applied Geophysics, v. 157, p. 957–976.

Waythomas, C.F., 2000, Reevaluation of tsunami formation by debris avalanche at Augustine Volcano, Alaska: Pure and Applied Geophysics, v. 157, p. 1145–1188.

Waythomas, C.F., and Waitt, R.B., 1998, Preliminary volcano-hazard assessment for Augustine Volcano, Alaska: U.S. Geological Survey Open-File Report 98-0106, 39 p.

Waythomas, C.F., Watts, P., and Walder, J.S., 2006, Numerical simulation of tsunami generation by cold volcanic mass flows at Augustine Volcano, Alaska: Natural Hazards and Earth System Sciences, v. 6, p. 671–685.

Wesson, R.L., Boyd, O.S., Mueller, C.S., Bufe, C.G., Frankel, A.D., and Petersen, M.D., 2007, Revision of time-independent probabilistic seismic hazard maps for Alaska: U.S. Geological Survey Open-File Report 2007–1043, 33 p.

Zimbelman, D.R., Watters, R.J., Firth, I.R., Breit, G.N., and Carrasco-Núñez, G., 2004, Stratovolcano stability assessment methods and results from Citlaltépetl, Mexico: Bulletin of Volcanology, v. 66, no. 1, p. 66–79.

> *This Morning at 8.[15] o'clock 4 Tidal Waves flowed one following the other into the shore, the sea rising 20 feet above the usual Level. The air became black and foggy, and it began to thunder; it began to rain a finely Powdered Brimstone Ashes, which lasted for about 10 Minutes, and which covered all the parts of Land to a depth of over 1/4 of a inch, clearing up at 9 o'clock A.M. Cause of occurrence: Eruption of the active Volcano at the Island of Chonoborough. Rain of Ashes commencing again at 11. o'clock A.M. and lasting all day.* [simplified]

George Davidson, a 16-year veteran of mapping Alaska's coast, summarizes accounts of witnesses to Augustine's effects near English Bay (Davidson, 1884):

> *About eight o'clock on the morning of Oct. 6, 1883, parties at English Harbor heard a heavy report to windward. Dense volumes of smoke were rolling out of the summit of St. Augustin, moving north-eastward, and a column of white vapor arose from the sea near the island. Fine pumice-dust soon began to fall. About twentyfive minutes past eight A.M., a great 'earthquake wave' came like a wall of water. It carried off all the fishingboats from the point, and deluged the houses. Fortunately it was low water, or all of the people at the settlement must inevitably have been lost.* [simplified]

Davidson's eruption "smoke" from Augustine at about 8 o'clock concludes in the ACC logbook entry: ashfall at 11—three hours for the cloud to drift 85 km east-northeast to English Bay. A tide-gauge marigram at St. Paul (Kodiak) harbor also record an explosion and the tsunami of contemporary accounts. Superimposed on a tidal oscillation of 1.8 m are two high-frequency signals: an air-wave arrival at 8:31 a.m. and tsunami arrival at 11:00 (fig. 14). The air wave records an explosive eruption. At sound speed (about 331 m/s), it covers the 185 km air distance in about 9.3 minutes, implying eruption at Augustine about 8:22.

The volcano continued in intermittent eruption for months. In a late-1884 letter, Davidson reported that in June 1884 an ACC captain sailed past Augustine Island and saw:

> *From the summit a great slide over half a mile broad towards the rocky boat harbor on the north. Material had poured to the base of the mountain and filled the harbor.* [simplified]

Burr Point Debris Avalanche

Steep hummocks as high as 30 m about Burr Point (fig. 12) resemble the debris avalanche off Mount St. Helens in May 1980. A sharp levee of andesite blocks marks the avalanche's west margin. Brecciated andesite constitutes the hummocks, individual blocks to 5 and 10 m, one slab 25 m long, all in a matrix of pulverized andesite rich in very angular clasts. Several blocks of loose sintered spatter and fragile fall pumice rafted to the coast intact.

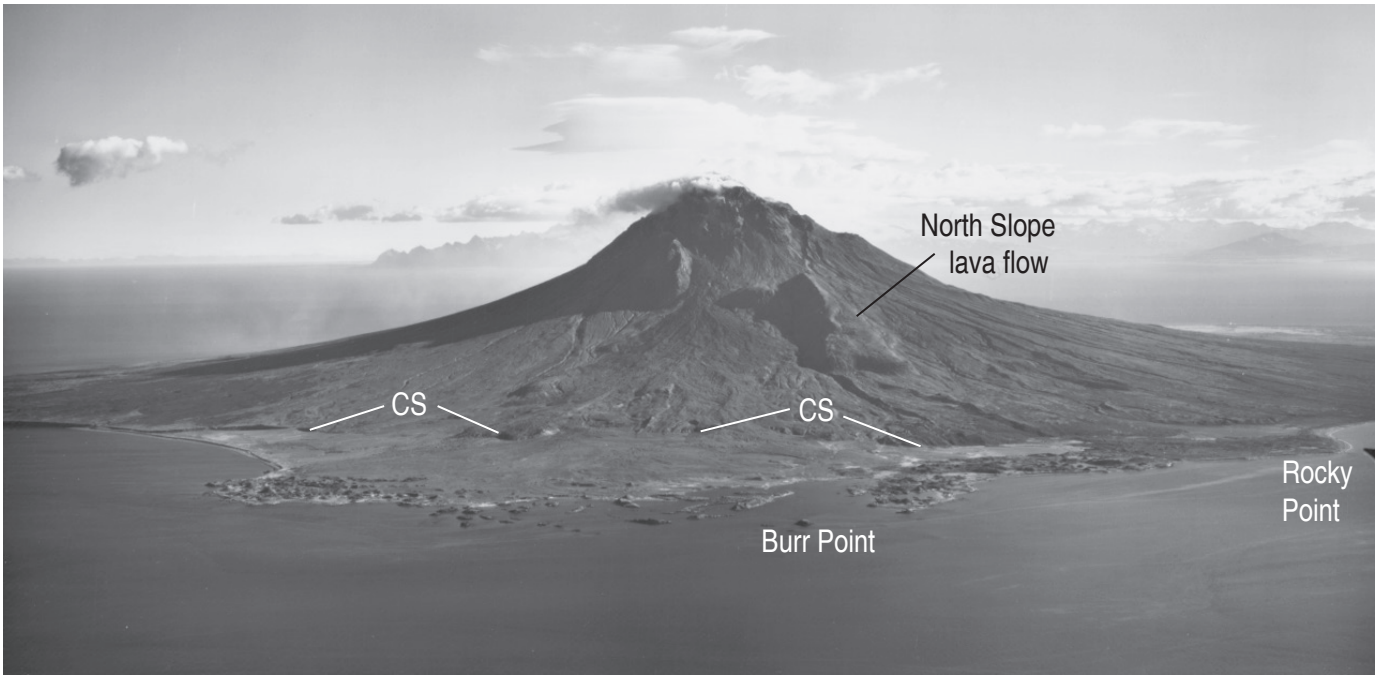

Figure 12. Distant oblique-aerial view of Augustine from the north showing hummocky deposit about Burr Point deposited by landslide in October 1883. This avalanche overrode the cliffed shoreline (CS) and entered the sea. Debris avalanche is in turn overlain by light-colored pyroclastic-flow debris of 1883, overlain upslope by small flows of 1935 and 1963–64. Smaller late-prehistoric Rocky Point avalanche lies just west (right). North Slope lava flow apparently erupted shortly after Rocky Point avalanche, long before Burr Point avalanche. Summit is 1964 dome. USGS photograph by Austin Post, September 3, 1966.

A former high seacliff on Augustine's north-northeast coast (figs. 5, 12) was overridden by the avalanche, which then plowed into the sea. Clear on 1960s' photographs, the cliff grows obscure as 1976 and 1986 pyroclastic flows bury the old scarp. Burr Point's islands extend to 2 ⅔ km, and submarine hummocks 4 km, beyond the old seacliff (fig. 6).

Its hummocks nearly devoid of vegetation and the many islands only meagerly carved back into seacliffs show Burr Point to be much younger than West Island. Rocky Point's thicker soil and offshore parts reduced to rocky shoals also show Burr Point's relative youth. Burr Point hummocks are overlain by soil containing the 1912 Katmai ash underlain by gray 1883 ash. Inland the gray ash is overlain by pyroclastic flow later in the 1883 eruption.

Coastal hummocks draped high above storm high water by mud containing exotic crystalline-rock pebbles enclose marine shells dating to 6,210–7,170 ^{14}C yr B.P. (fig. 15). To have scraped up such mud the avalanche must have plowed into the bay at high speed.

Pyroclastic Flow and Surge, and Lava Dome

Burr Point avalanche is buried upslope by laminated medium sand overlain by thick massive pebbly medium sand cut by openwork gravel pipes that had conveyed steam up from underlying wet mud. Pyroclastic surge apparently came after the avalanche. Then one or more hot pyroclastic flows filled a watery low behind the avalanche hummocks.

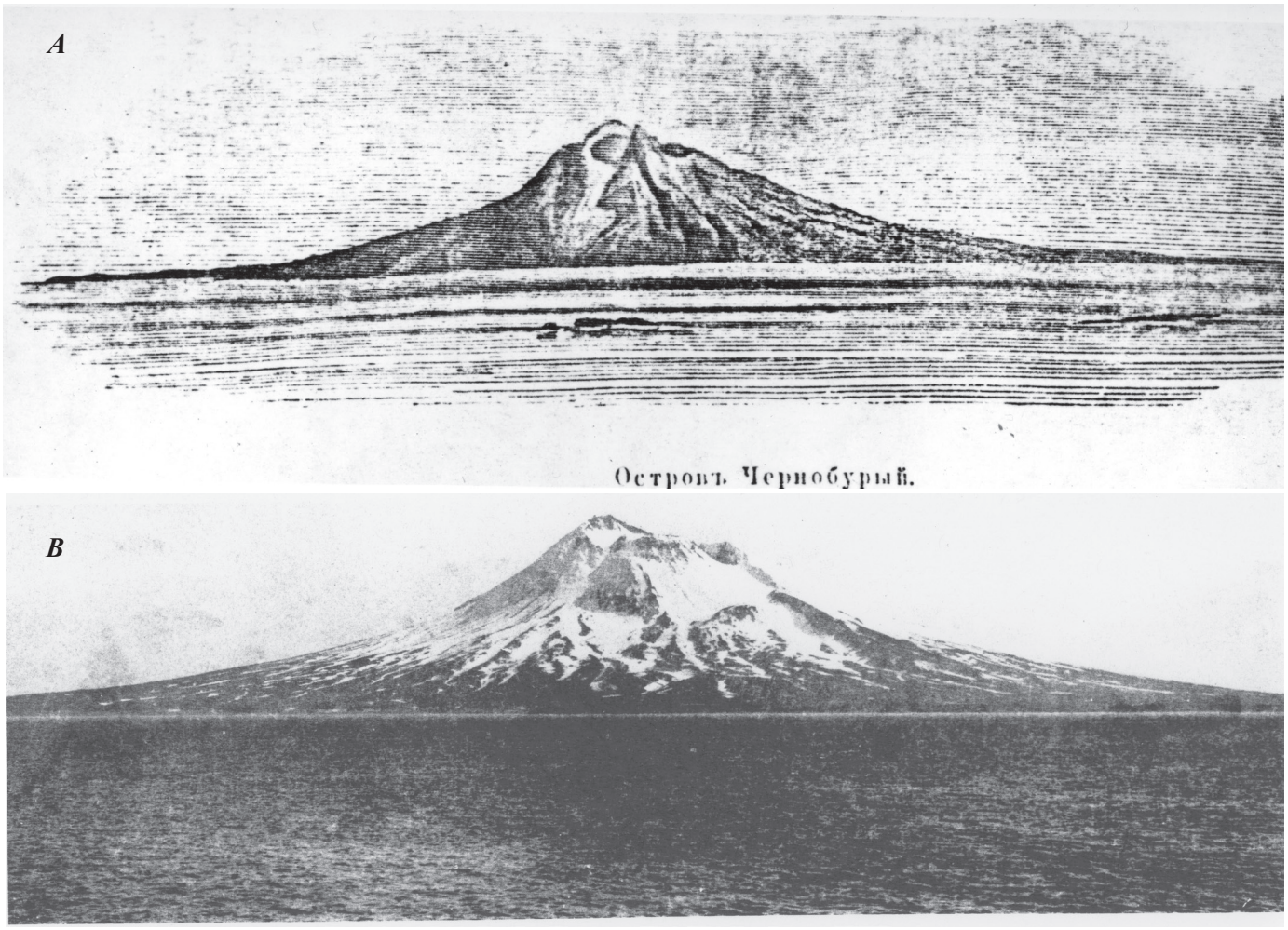

Figure 13. Augustine Volcano, Alaska, showing large-scale effects to summit area by 1883 eruption. *A*, Drawing by Doroshin (1870) showing spine, view from northeast. Bump on right horizon and downslope right of spine seems to be North Slope lava flow. Compared to later photographs, the northeast shoreline of Augustine shown here is less extended: Burr Point deposit does not yet exist. *B*, Photograph taken 1909 from similar northeast perspective by John Thwaites. Since 1870 the former spine and part of upper north flank disappeared, replaced by a large lava dome. Contrasting to Doroshin's drawing, Burr Point now exists.

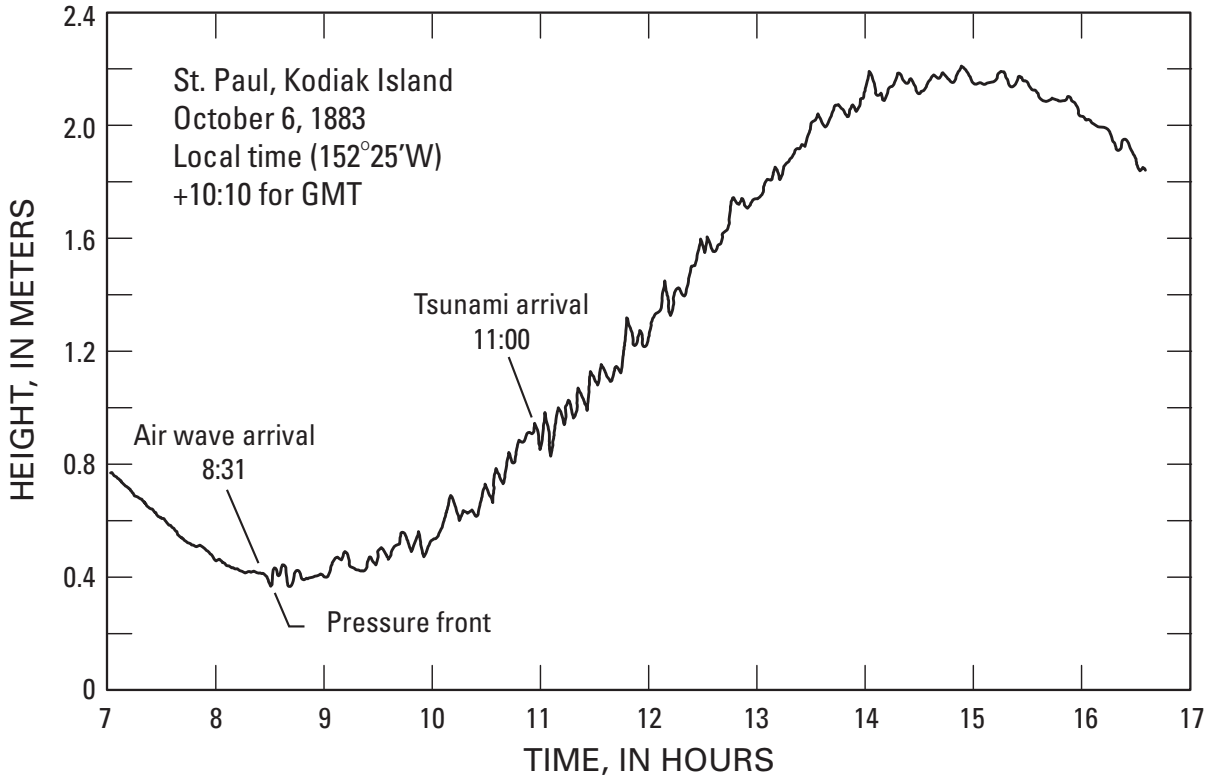

Figure 14. Tide-gauge marigram from St. Paul (Kodiak), Alaska, on October 6, 1883. It shows arrivals of wave train of air wave and of tsunami from Augustine, both superimposed on a tidal cycle of amplitude 1.8 m. Marigram from US Coast and Geodetic Survey archives (see Lander, 1996, p. 49 and fig. 16). The gauge was at Kodiak (St. Paul) Harbor at longitude 152°25′ W). Time is local sun time (before standardized time zones in 1884). For GMT add about 10 hours, 10 minutes. First motion in tide guage for air-pressure wave (depressing sea surface) is negative but for tsunami (raising sea surface) is positive. Lander (1996, figs. 48–90) shows many marigrams and interprets tsunami waves on them.

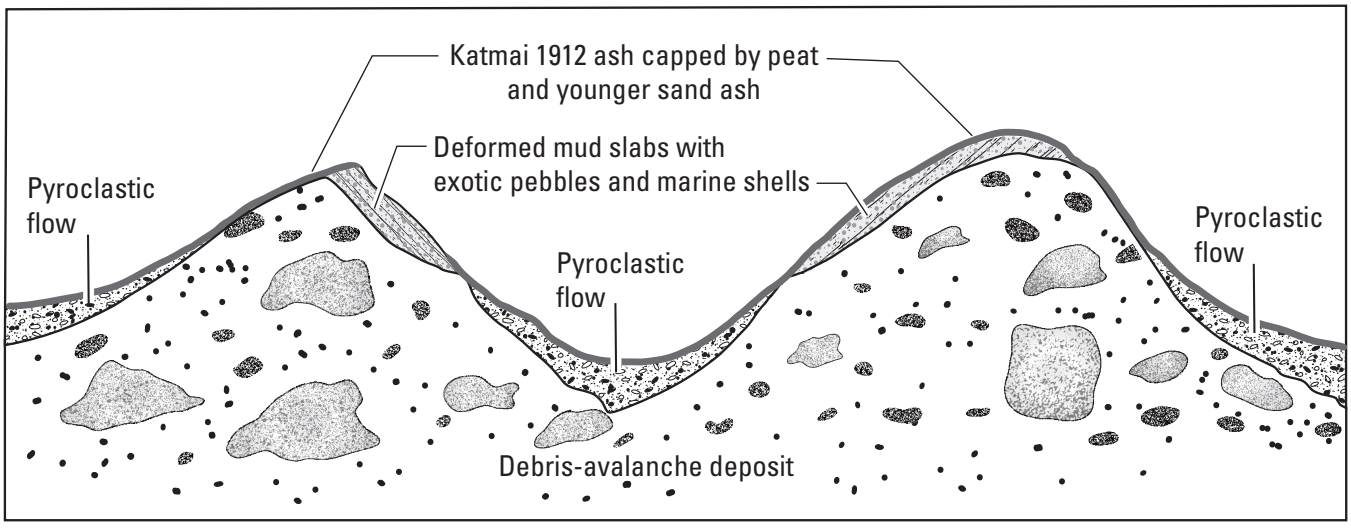

Figure 15. Schematic sketch of stratigraphic relations atop 1883 hummocks east of Burr Point. Bouldery debris avalanche is overlain by pyroclastic flow and by Katmai 1912 silt ash and younger sand ashes interlayered with peat. Deformed slabs (lined) of compact, fissile mud containing marine shells and rounded small pebbles of diverse exotic lithology drape over some hummocks. Marine shells (see explanation in text) from these slabs are radiocarbon dated at 6,210 and 7,170 yr B.P.

A broad lava dome that grew in the subsummit avalanche scar shows on photographs taken before 1963 (figs. 13*B*, 16). The 1883 crater still steamed profusely and rocks rolled off in 1895, as if the dome remained active (Becker, 1898). This dome disappeared beneath the 1976 lava dome.

1935 and 1963–64 Eruptions

Photographs from 1935 show a steaming dome draping west-southwest off the summit cone. Aerial photographs in the 1940s to 1960s and Bob Detterman's 1967 fieldwork also distinguish this dome. Rubble downslope contains angular boulders to 6 m where 1935 photos show light-toned debris recently shed from the dome. Remnants of the 1935 dome form a point just north-northwest of the summit (fig. 5).

From his 1967 visit, Detterman (1968) described the 1963–64 eruption, the summit dome steaming through 1966. The 1964 dome crowning the old summit complex drapes down to the south (figs. 5, 7). Downslope the bouldery andesite rubble includes clasts as large as 7 m on a debris fan whose intricate levees reveal emplacement by repeated lithic pyroclastic flows. Scattered large angular blocks lie in areas of 1964 ballistic fall denoted by Detterman (1968).

1976 and 1986 Eruptions

Augustine's 1976 eruption, better chronicled than earlier ones (Johnston, 1978; Kienle and Shaw, 1979), explosively shed pumiceous pyroclastic flows onto several flanks, especially north, in late January and early February. A large andesite summit dome emerged in February, grew rapidly in April, and tapered off into summer. It buried the 1883 dome and part of the 1935 dome. Its steep north edge repeatedly sloughed lithic pyroclastic flows.

North-flank 1976 pumiceous pyroclastic flows approached and reached the sea. Overlapping pumiceous flows end in intricately lobate marginal scarps and contain large pumice blocks and banded breadcrust bombs. Shed later from the growing dome, lithic flows with huge blocks but

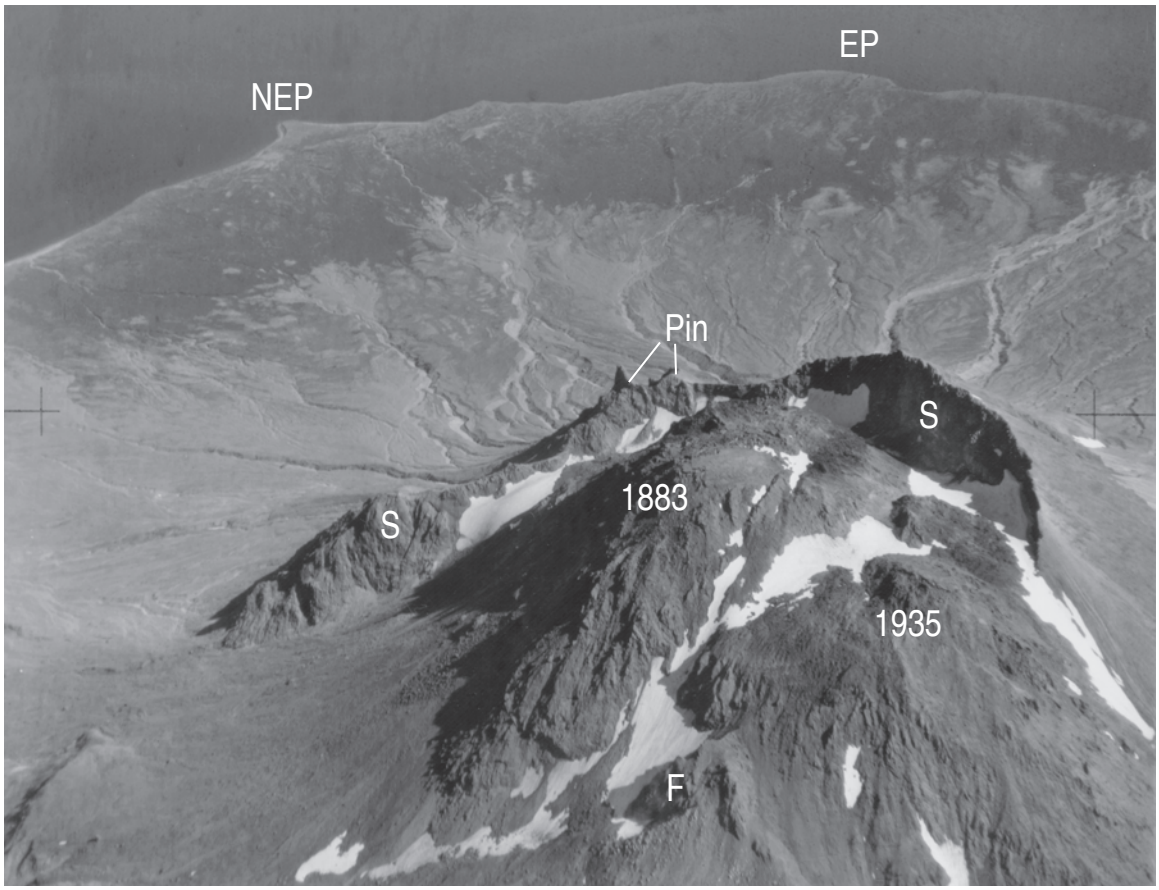

Figure 16. Oblique-aerial photograph eastward of Augustine Volcano before 1963–64 eruption showing 1883 and 1935 domes and prehistoric summit-dome complex (S) and dome F (dome P, below F, is out of shot). Arcuate scarp behind 1883 dome is scar left by 1883 landslide that cut into the composite summit dome including Pinnacles area (Pin). The coastal landmarks are Northeast Point (NEP) and East Point (EP). USGS photograph by Austin Post, August 24, 1960.

little pumice spread less far. Pumiceous flows also descended swales and gullies on other flanks across older fragmental debris, following some gullies nearly to the coast (fig. 5). A late-January surge reached Burr Point and offshore. It ripped into a research hut, inside burning mattresses and melting plastic, simulated in a lab oven at 500–700°C (Johnston, 1978; Kamata and others, 1991; Waitt and Begét, 2009).

Augustine's eruptions between late March and late August 1986 sent scores of pyroclastic flows down its north and northeast flanks. Some early pumiceous pyroclastic flows melted snow to transform into watery floods that left small bars of gravel and lags of boulders or graded down gullies into lahars. An andesite lava dome extruding near the summit incorporated the 1976 dome (fig. 17) (Yount and others, 1987; Swanson and Kienle, 1988). As the new dome grew between late April and late August, parts of it repeatedly collapsed to form small billowing pyroclastic flows that smeared coarse andesite rubble down the north and northeast flanks.

2006 Eruption

The 2006 eruption spewed small flows onto all flanks except the west (Vallance and others, this volume). On January 28, 2006, a pyroclastic flow of dense pumice swept down to the lower north flank and filled the shallow pond there. In winter 2006, a dome grew at the summit, filling the subsummit moat north of the 1986 dome and covering that dome and draping new stiff lava flows down the upper north and northeast flank. These and small lithic pyroclastic flows spalling from the lava flows expanded until the end of March 2006. Simplified here as figure 5, Waitt and Begét's (2009, plate 1) geologic map is as plotted before the 2006 eruption.

High-Energy Flows from an Island

Pyroclastic Density Current

Hot pyroclastic density currents (flows and surges) can move at 280 km/hr and cross water. Surges crossed water lethally during 1902 eruptions of Mont Pelée and La Soufrière and during 1911 and 1965 eruptions at Taal in the Philippines (Anderson and Flett, 1903; Moore and others, 1966; Blong, 1984; Scarth, 2002). Many ashy flows and surges of the last 2,200 years lie at Augustine's coast. Clearly they sweep into the sea from time to time.

Figure 17. View southward of 1986 dome and lava-flow tongue at its base. Photograph mid-July 1986 by Jürgen Kienle, University of Alaska Geophysical Institute.

A landslide taking a volcano's summit will depressurize intruding magma and hot groundwater. These can explode as at Mount St. Helens in May 1980 when the fountaining gas-rock mixture collapsed into a ground-hugging hot surge (Waitt, 1981). But of Augustine's 12 debris avalanches in the past 2,300 years, only West Island about 370 yr B.P. clearly includes a large ground surge.

Debris Avalanche

Augustine's many hummocky boulder diamicts around its coasts originated as debris avalanches from collapsing summit domes. Bulk volume of Burr Point avalanche beyond the former coast is about 0.25 km^3 and of West Island avalanche about 0.4 km^3. On southwest West Island, the planed-off hummocks and lag boulders record a great sweep of avalanche-displaced seawater. The mud slabs with marine shells draping hummocks at Burr Point show that the 1883 avalanche also crashed into the sea violently. Many earlier Augustine avalanches of similar volumes rode far seaward, indicating their high speed into seawater.

Tsunami

At least twelve debris avalanches off Mount Augustine in the past 2,300 years entered the sea, that in 1883 (Burr Point) generating witnessed tsunami. Many historical debris avalanches off alpine mountains or volcanoes have run into water fast enough to generate large waves on distant shorelines (Waitt and Begét, 2009, table 4). Augustine Island gives evidence that two of its debris avalanches initiated tsunami: West Island about 370 yr B.P. and Burr Point in 1883.

The shores of lower Cook Inlet bear sporadic and sparse evidence of tsunami. On the mainland north-northeast of Augustine, sand 2 m above high tide bearing beach cobbles and logs overlies 300-yr-B.P. Iliamna eruptive deposits, and trees rooted deeper show a tree-ring perturbation at A.D. 1883 (fig. 1*A*) (Anders and Begét, 1999). An apparent 1883 tsunami deposit crops out 1½ m above spring high tide on the sand spit that guards Nanwalek (English Bay) harbor. Overlying a brown soil, sand containing beach pebbles and cobbles washed upslope (fig. 18). Gray ash atop the pebbles is surely the ashfall from Augustine in October 1883 of the contemporary accounts. This is capped by the white Katmai ash of 1912 (Begét and Kowalik, 2006, fig. 5; Begét and others, 2008; Waitt and Begét, 2009).

Possible prehistoric tsunami deposits—beds of sand bearing rounded cobbles—lie within thick peat beds 5 m above high tide near Nanwalek and Seldovia (Begét and others, 2008). Enclosing peat dating to 1,620–1,650 yr B.P. approximately coincides with Augustine's Northeast Point debris avalanche (fig. 5; table 1). A likely tsunami deposit

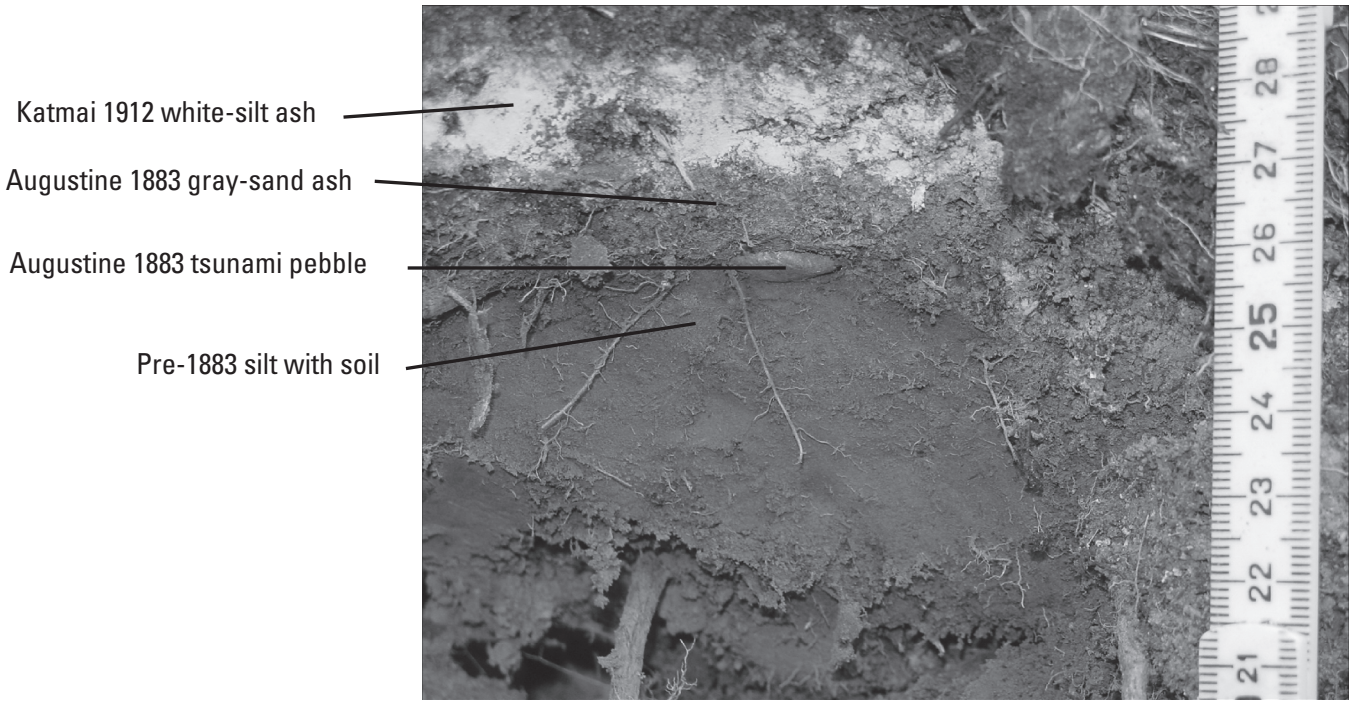

Figure 18. View of 1883 tsumani and ashfall deposits near Nanwalek (in 1883 English Bay). Overlying a brown soil are beach pebbles transported up to 1.5 meters above high-tide level, evidently by tsunami on October 6, 1883. Above the pebbles lies 1.5 cm of fine-sand ash, evidently of 1883 ashfall deposited October 6–7, 1883. Overying that is Katmai 1912 white-silt ash. Scale numbered in centimeters. Photograph by J.E. Begét, University of Alaska, Fairbanks. Begét and Kowalik (2006, fig. 5) show a different view of this stratigraphy.

lies at Point Bede on lower Kenai Peninsula (fig. 1*A*)—angular large boulders thrown 5–10 m back from a seacliff 1 to 2 m above high tide. Atop the boulders and beneath Katmai 1912 ash lie 2–4 sand-silt ashes, showing the boulders were cast up several centuries ago.

Summary

Augustine began erupting before or during the late Wisconsin. Several south-flank exposures reveal sporadic middle to late Holocene eruptions of pumiceous flows and coarse pumiceous tephra. Between 2,200 and 390 B.P., six eruptions deposited coarse-pumice tephra, an average one every 300–360 yr. Countless smaller eruptions deposited many thinner and finer ash layers.

The dominant style over time seems to be growth of steep summit domes, eventually truncated by collapse into a debris avalanche—one every 180–200 years average. Eruptions of coarse pumiceous tephra and significant pyroclastic flows average once every three centuries or so.

Augustine's late Holocene debris avalanches are many, but an attending Mount St. Helens-like surge seems rare. A surge deposit does overlie bits of West Island avalanche. Whether most debris avalanches came during or between eruptions is unclear. That some avalanches contain prismatically jointed andesite reveals hot rock in the summit dome at the time. But in only a few of the documented stratigraphic sections does a coarse tephra immediately overlie a debris avalanche. Spotty tephra G overlies nearly directly the uppermost of the East Point avalanches, tephra I overlies Southeast Point avalanche (fig. 9), and tephra C immediately overlies South Point avalanche. These suggest but by do not prove that the decapitations of the summit dome uncorked substantial eruptions. Apparently the 1883 avalanche immediately preceded eruptions of sand-sized tephra. An 1883-like avalanche was a worry just before the 2006 eruption. But no serious swelling appeared like that preceding the May 1980 landslide off Mount St. Helens.

The seven historical eruptions between 1812 and 2006 have yielded no tephras comparable to the six thick and coarse prehistoric pumiceous ones. Pumiceous flows on the north flank in the 1976 and 1986 eruptions did build fans as thick as some of those in prehistoric eruptions on other flanks.

The waves as high as 6 or 7 m at English Bay in October 1883 originated when a moderate-volume avalanche swept into the shallow sea. Augustine's summit has since grown back wider and taller than it was just before that slide. The 1883 avalanche occurred during a falling low tide in a sparsely populated region. Were a large debris avalanche off Augustine to plunge into the sea during intermediate or high tide, consequent tsunami in coastal areas of lower Cook Inlet would likely be larger and far more damaging.

References Cited

Alaska Commercial Company, 1883 [unpublished], Record Books for English Bay Station: Fairbanks, University of Alaska library Archives, Box 10 (May 15, 1883–July 1884).

Anders, A.M., and Begét, J.E., 1999, Giant landslides and coeval tsunamis in lower Cook Inlet, Alaska [abs.]: Geological Society of America Abstracts with Programs, v. 31, no. 7, p. A48

Anderson, T., and Flett, 1903, Report on the eruptions of the Soufrière in St. Vincent, and on a visit to Montagne Pelée in Martinique: Philosophical Transactions of the Royal Sociey of London, Ser. A, v. 200, p. 353–553.

Beaglehole, J.C., ed., 1967, The voyage of the *Resolution* and *Discovery* 1776–1780—The Journals of Captain James Cook on his Voyages of Discovery: Hakluyt Society, Cambridge University Press, 718 p.

Becker, G.F., 1898, Reconnaissance of the gold fields of southern Alaska, with some notes on general geology: U.S. Geological Survey 18th Annual Report, pt. 3, p. 28–58.

Begét, J.E., and Kienle, J., 1992, Cyclic formation of debris avalanches at Mount St. Augustine volcano: Nature, v. 356, p. 701–704.

Begét, J.E., and Kowalik, 2006, Confirmation and calibration of computer modeling of tsunamis produced by Augustine Volcano, Alaska: Science of Tsunami Hazards, v. 24, p. 257–266.

Begét, J.E., Gardner, C.A., and Davis, K., 2008, Volcanic tsunamis and prehistoric cultural transitions in Cook Inlet, Alaska: Journal of Volcanology and Geothermal Research, v. 176, p. 377–386.

Blong, R.J., 1984, Volcanic hazards—a sourcebook on the effects of eruptions: Sydney, Academic Press, 424 p.

Coombs, M.L., Bull, K.F., Vallance, J.W., Schneider, D.J., Thoms, E.E., Wessels, R.L., and McGimsey, R.G., 2010, Timing, distribution, and volume of proximal products of the 2006 eruption of Augustine Volcano, *in* Power, J.A., Coombs, M.L., and Freymueller, J.T., eds., The 2006 eruption of Augustine Volcano, Alaska: U.S. Geological Survey Professional Paper 1769 (this volume).

Daley, E.E., 1986, Petrology, geochemistry, and the evolution of magmas from Augustine volcano, Alaska: Fairbanks, University of Alaska, M.S. thesis, 69 p.

Davidson, G., 1884, Notes on the eruption of Mount St. Augustine, Alaska, October 6, 1883: Science, v. 3, no. 54, p. 186–189.

Detterman, R.L., 1968, Recent volcanic activity on Augustine Island, Alaska: U.S. Geological Survey Professional Paper 600-C, p. 126–129.

Detterman, R.L., and Hartsock, J.K., 1966, Geology of the Iniskin-Tuxedni region, Alaska: U.S. Geological Survey Professional Paper 512, 78 p. and geologic map, scale 1:63,360.

Detterman, R.L., and Jones, D.L., 1974, Mesozoic fossils from Augustine Island, Cook Inlet, Alaska: American Association of Petroleum Geologists Bulletin, v. 58, p. 868–870.

Doroshin, Petr, 1870, Some volcanoes, their eruptions, and earthquakes in the former Russian holdings in America: Verhandlungen der Russisch-Kaiserlichen Mineralogischen Gesellschaft zu St. Petersburg, Zweite Serie, Fünfter Rand, p. 25–44 (in Russian).

Glicken, H., 1996, Rockslide–debris avalanche of May 18, 1980, Mount St. Helens volcano, Washington: U.S. Geological Survey Open-File Report 96-677, 90 p.

Glicken, H., 1998, Rockslide–debris avalanche of May 18, 1980, Mount St. Helens volcano, Washington: Bulletin of the Geological Survey of Japan, v. 49, p. 55–106 and 10 map plates.

Hamilton, T.D., and Thorson, R.M., 1983, The Cordilleran ice sheet in Alaska, *in* Porter, S.C., ed., vol. 1, The late Pleistocene, *in* Wright, H.E., Jr., ed., Late Quaternary environments of the United States: Minneapolis, University of Minnesota Press, p. 38–52.

Johnston, D.A., 1978, Volatiles, magma mixing, and the mechanism of eruption of Augustine volcano, Alaska: Seattle, University of Washington, Ph.D. dissertation, 177 p.

Jones, D.L., and Clark, S.H.B., 1973, Upper Cretaceous (Maestrichtian) fossils from the Kenai-Chugach Mountains, Kodiak and Shumagin Islands, southern Alaska: U.S. Geological Survey Journal of Research, v. 1, 125–136.

Kamata, H., Johnson, D.A., and Waitt, R.B., 1991, Stratigraphy, chronology, and character of the 1976 pyroclastic eruption of Augustine volcano, Alaska: Bulletin of Volcanology, v. 53, p. 407–419.

Kienle, J. and Shaw, G.E., 1979, Plume dynamics, thermal energy, and long-distance transport of vulcanian eruption clouds from Augustine volcano, Alaska: Journal of Volcanology and Geothermal Research, v. 6, p. 139–164.

Kienle, J., and Swanson, S.E., 1983, Volcanism in the eastern Aleutian arc—late Quaternary and Holocene centers, tectonic setting and petrology: Journal of Volcanology and Geothermal Research, v. 17, p. 393–432.

Kienle, J., and Swanson, S.E., 1985, Volcanic hazards from future eruptions of Augustine volcano, Alaska: Fairbanks, University of Alaska Geophysical Institute, document R-275, 126 p. and map.

Lamb, W.K., ed., 1984, George Vancouver, A Voyage of Discovery to the North Pacific Ocean and round the world 1791–1795, v. 4: London, Hakluyt Society, no. 166.

Lander, J.F., 1996, Alaskan tsunamis 1737–1996: National Oceanographic and Atmospheric Administration (NOAA), National Geophysical Data Center (Boulder, Colo.), Geophysical Research Document 31, 195 p.

Larsen, J.F. Nye, C.J., Coombs, M.L., Tilman, M., Izbekov, P., and Cameron, C., 2010, Petrology and geochemistry of the 2006 eruption of Augustine Volcano, *in* Power, J.A., Coombs, M.L., and Freymueller, J.T., eds., The 2006 eruption of Augustine Volcano, Alaska: U.S. Geological Survey Professional Paper 1769 (this volume).

LeBas, M.J., and Streckeisen, R.W., 1991, The IUGS systematics of igneous rocks: Journal of the Geological Society of London, v. 148, p. 825–833.

Magoon, L.B., Adkison, W.L., and Egbert, R.M., 1976, Map showing geology, wildcat wells, Tertiary plant fossil localities, K-Ar age dates, and petroleum operations, Cook Inlet area, Alaska: U.S. Geological Survey Miscellaneous Investigations Series Map I-1019.

Moore, J.G., Kazuaki, N., and Alcaraz, A., 1966, The 1965 eruption of Taal volcano: Science, v. 151, p. 955–960.

Riehle, J.R., Waitt, R.B., Meyer, C.E., and Calk, L.C., 1998, Age of formation of Kaguyak Caldera, eastern Aleutian arc, Alaska, estimated by tephrochronology: U.S. Geological Survey Professional Paper 1595, p. 161–168.

Roman, D.C., Cashman, C.V., Gardner, C.A., Wallace, P.J., and Donovan, J.J., 2006, Storage and interaction of compositionally heterogeneous magmas from the 1986 eruption of Augustine Volcano, Alaska: Bulletin of Volcanology, v. 68, p. 240–254.

Scarth, A., 2002, La Catastrophe—the eruption of Mount Pelée, the worst volcanic disaster of the 20th century: Oxford University Press, 246 p.

Siebert, L., Glicken, H., and Kienle, J., 1989, Debris avalanches and lateral blasts at Mount St. Augustine volcano, Alaska: National Geographic Review, v. 5, p. 232–249.

Siebert, L., Begét, J.E., and Glicken, H., 1995, The 1883 and late-prehistoric eruptions of Augustine volcano, Alaska: Journal of Volcanology and Geothermal Research, v. 66, p. 367–395.

Swanson, S.E., and Kienle, J., 1988, The 1986 eruption of Mount St. Augustine—field test of a hazard evaluation: Journal of Geophysical Research, v. 93, p. 4500–4520.

Vallance, J.W., Bull, K.F., and Coombs, M.L., 2010, Pyroclastic flows, lahars, and mixed avalanches generated during the 2006 eruption of Augustine Volcano, *in* Power, J.A., Coombs, M.L., and Freymueller, J.T., eds., The 2006 eruption of Augustine Volcano, Alaska: U.S. Geological Survey Professional Paper 1769 (this volume).

Voight, B., Janda, R.J., Glicken, H., and Douglass, P.M., 1983, Nature and mechanics of the Mount St. Helens rockslide avalanche of 18 May 1980: Geotechnique, v. 33, p. 243–273.

Waitt, R.B., 1981, Devasting pyroclastic density flow and attendant air fall of May 18—stratigraphy and sedimentology of deposits, *in* Lipman, P.W., and Mullineaux, D.R., eds., The 1980 eruptions of Mount St. Helens, Washington: U.S. Geological Survey Professional Paper 1250, p. 439–458.

Waitt, R.B., and Begét, J.E., with contributions by Juergen Kienle, 1996, Provisional geologic map of Augustine Volcano, Alaska: U.S. Geological Survey Open-File Report 96-516, 44 p., map scale 1:25,000.

Waitt, R.B., and Begét, J.E., 2009, Volcanic processes and geology of Augustine Volcano, Alaska: U.S. Geological Survey Professional Paper 1762, 78 p. and 2 map plates.

Yount, M.E., Miller, T.P., and Gamble, B.M., 1987, The 1986 eruptions of Augustine Volcano, Alaska—hazards and effects: U.S. Geological Survey Circular 998, p. 4–13.

This page intentionally left blank

The 2006 Eruption of Augustine Volcano, Alaska
Power, J.A., Coombs, M.L., and Freymueller, J.T., editors
U.S. Geological Survey Professional Paper 1769

Chapter 14

Preliminary Slope-Stability Analysis of Augustine Volcano

By Mark E. Reid[1], Dianne L. Brien[1], and Christopher F. Waythomas[2]

Abstract

Augustine Volcano has been a prolific producer of large debris avalanches during the Holocene. Originating as landslides from the steep upper edifice, these avalanches typically slide into the surrounding ocean. At least one debris avalanche that occurred in 1883 during an eruption initiated a far-traveled tsunami. The possible occurrence of another edifice collapse and ensuing tsunami was a concern during the 2006 eruption of Augustine. To aid in hazard assessments, we have evaluated the slope stability of Augustine's edifice, using a quasi-three-dimensional, geotechnically based slope-stability model implemented in the computer program SCOOPS. We analyzed the effects of topography, variations in rock strength, and earthquake-induced strong ground motion on the relative stability of millions of potential large (>0.1 km^3 volume) slope failures throughout the edifice.

Preliminary results from pre-2006 topography provide three insights. First, the predicted stability of all parts of the upper edifice is approximately the same, suggesting an equal likelihood of slope failure, in agreement with geologic observations that debris avalanches have swept all sectors of the volcano. Second, the least stable (by a small amount) sector is on the east flank where a debris avalanche would flow into deeper ocean water and a resulting tsunami would be directed toward the southwestern part of the Kenai Peninsula. Third, most model scenarios predict stable edifice slopes, and only scenarios assuming extensive weak rocks and moderate to strong ground shaking predict potential large collapses. Because other transient triggering mechanisms, such as shallow magma intrusion, may be needed to instigate slope instability, monitoring ground deformation and seismicity could help short-term forecasting of impending edifice failure.

[1]U.S. Geological Survey, 345 Middlefield Road, MS 910, Menlo Park, CA 94025.

[2]Alaska Volcano Observatory, U.S. Geological Survey, 4200 University Drive, Anchorage, AK 99508.

Introduction

Augustine Volcano, an island volcano near the mouth of Cook Inlet, Alaska (fig. 1) composed primarily of multiple lava domes, has produced a remarkable series of large debris avalanches over the past 3,500 years. These debris avalanches, believed to initiate as massive landslides emanating from the flanks or summit of the edifice (Siebert and others, 1989; Begét and Kienle, 1992; Siebert and others, 1995), typically travel into the surrounding ocean (Waythomas and Waitt, 1998; Waythomas and others, 2006). Previous investigators have hypothesized that tsunamis occur when debris avalanches enter the sea during eruptions of the volcano (Kienle and Swanson, 1985; Kienle and others, 1987; Begét and Kienle, 1992; Siebert and others, 1995; Begét and Kowalik, 2006; Begét and others, 2008). A debris avalanche generated during the 1883 eruption of Augustine is believed to have caused a tsunami that struck the village of English Bay (now called Nanwalek), about 80 km east of the volcano (Davidson, 1884; Kienle and others, 1987; Siebert and others, 1995; Lander, 1996). Augustine is one of the most historically active volcanoes in the eastern Aleutian Arc (Simkin and Siebert, 1994; Miller and others, 1998), and its renewed eruptive activity in 2006 prompted concerns about a potential edifice collapse and subsequent tsunami.

During the 2006 eruption of Augustine, we performed a preliminary slope-stability analysis of the upper edifice. Numerous factors can affect the potential instability of volcanic edifices (Voight and Elsworth, 1997), including steep slopes, weakened rocks, strong earthquake shaking, shallow magma intrusion, elevated pore-fluid pressures induced by rain or snowmelt infiltration, or thermal fluid pressurization from intruding magma (Reid, 2004). Most of these factors are poorly known at Augustine as well as at other volcanoes. The 1883 edifice collapse occurred early in an eruption, and geologic evidence indicates the West Island debris avalanche occurred during an earlier eruption about 450 yr B.P., but it is uncertain whether all previous large slope failures were associated with eruptions. Rather than speculate on a myriad of destabilization scenarios, our preliminary analysis focused on two controls that are better known at Augustine: stresses

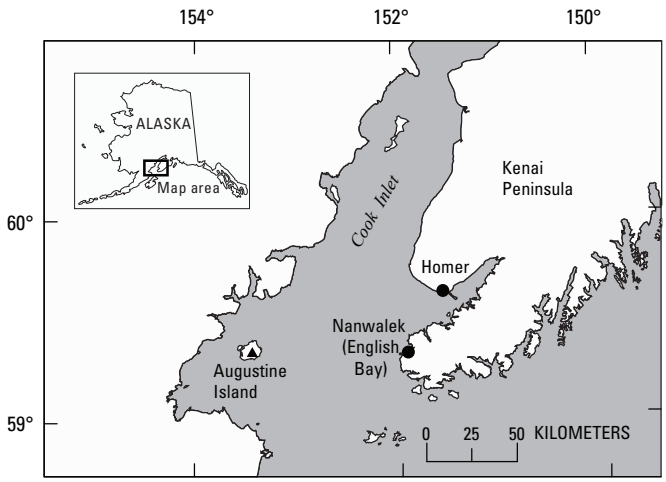

Figure 1. Southern Alaska, showing locations of Augustine Island, Cook Inlet, towns of Homer and Nanwalek (English Bay), and part of the Kenai Peninsula.

induced by topography and transient stresses created by strong ground motion during large earthquakes, in both of which rock strength strongly modulates potential slope instability. We used a quasi-three-dimensional (3D) geotechnical method implemented in the computer program SCOOPS (Reid and others, 2000) to perform our slope-stability assessments. We focused on potentially large (>0.1 km^3 volume) slope failures (landslides) affecting pre-2006 topography.

Herein we present a brief history of past debris avalanches from Augustine Volcano to provide a context for our slope-stability analyses, a short summary of our quasi-3D analytical approach, and the results for six plausible scenarios examining the effects of rock strength and earthquake-induced strong ground shaking at Augustine. Our preliminary analysis for each scenario indicates the relative stability of all parts of the upper edifice, the predicted least stable regions, and the volumes associated with potential slope failures.

History of Debris Avalanches at Augustine Volcano

Geologic studies on Augustine Island have identified and named at least 12 large debris-avalanche deposits on the flanks of the volcano that are younger than about 3,500 years (Waitt and others, 1996; Waitt and Begét, 2009; Waitt, this volume), each of which may have generated a tsunami when it flowed into Cook Inlet (Kienle and others, 1987; Begét and Kienle, 1992). Deposits of the West Island and Burr Point debris avalanches (fig. 2; table 1) possess the hummocky surface morphology, large megaclast blocks, and poorly sorted, fines-poor composition of similar deposits at Mount St. Helens (Siebert, 1984; Glicken, 1991). All of the large debris-avalanche deposits recognized on Augustine Volcano extend to the coast (Waitt and others, 1996; Waitt and Begét, 2009; Waitt, this volume) and typically are well exposed in seabluffs and gullies. Submerged hummocky topography offshore indicates that several of these debris avalanches traveled an additional 4 to 6 km across the sea floor.

Radiocarbon dating of buried soils associated with tephra and debris-avalanche deposits allowed Begét and Kienle (1992), Waitt and others (1996), and Waitt and Begét (2009) to propose a chronology for debris-avalanche formation at Augustine over the past 3,500 years (table 1). Their chronology is based on stratigraphic relations among dated tephra layers that are diagnostic enough in the field that they can be readily identified as stratigraphic markers. The stratigraphic relations of the debris-avalanche deposits to major tephra units can thus be used to establish age control on the debris-avalanche deposits. Other than the 1883 Burr Point deposit, no debris-avalanche deposits at Augustine have been directly dated, and it is unclear how many of these deposits are contemporaneous with major tephra units.

The spatial distribution of debris-avalanche deposits on Augustine Island indicates that debris avalanches have swept all sectors of the island in the past (fig. 2; table 1). At least five debris avalanches have occurred on the north and west flanks of the volcano, five on the east and south flanks, one on the northeast flank, and one on the southwest flank. The three most recent debris avalanches, including the 1883 Burr Point debris avalanche, postdate tephra B (about 478–257 yr B.P.) and have all been directed north-northwestward. Because of the approximately clockwise migration of slope failures around the edifice over the past several thousand years, some researchers have postulated an increased likelihood of future slope failure in the northeast sector (Siebert and Begét, 2006). The youngest debris avalanche on the southeast flank is recorded by the Southeast Beach debris-avalanche deposit (Waitt and Begét, 2009) which predates tephra B and postdates tephra M (about 709–478 yr B.P.).

Generalized physical descriptions of the debris-avalanche deposits at Augustine are presented by Waitt and others (1996) and Waitt and Begét (2009). Most of these deposits are composed of poorly sorted dacitic or andesitic rubble and silt- to boulder-size material. Megaclasts as large as 30 m across occur in some of the deposits; these clasts are intact pieces of former summit domes that were not disaggregated during downslope transport. Some of the clasts exhibit minor hydrothermal alteration, but only the Yellow Cliffs deposit (fig. 2) contains abundant material hydrothermally altered to clay. This debris-avalanche deposit is the only one at Augustine that records a flank collapse associated with pervasive alteration of the edifice.

Estimated volumes of the debris-avalanche deposits vary but most exceed 0.1 km^3. Siebert and others (1995) and Waitt and Begét (2009) estimated volumes for the debris-avalanche deposits on the north and west flanks of the volcano (table 1). The 1883 Burr Point debris-avalanche deposit has

Table 1. Characteristics of large debris-avalanche deposits on Augustine Island.

[Modified from Siebert and others (1995) and Waitt and Begét (2009). Composite stratigraphy includes debris-avalanche deposits and dated tephra deposits. Recalibrated radiocarbon ages (in years) bracketing tephras from Waythomas (2000)]

Composite stratigraphy	Map unit (fig. 2)	Sector of island affected	Volume of deposit (km^3)	Composition
Burr Point (A.D. 1883)	83a	North-northeast	0.25 to 0.3	Andesite, some alteration
Rocky Point	Bar	North	0.15	Andesite
West Island + Grouse Point	Baw, Bag	Northwest	0.3 to 0.5	Andesite, dacite
		(257±18) Tephra B (478±27)		
Southeast Beach	MBas	Southeast		Andesite
		(478±27) Tephra M (709±23)		
Lagoon	CMal	West		Andesite
		(709±23) Tephra C (1,102±22)		
North Bench	IMan	North-northwest		Andesite
Long Beach	HCal	Southwest		Andesite
South Point	HCas	South		Andesite
		(1,102±22) Tephra H (1,552±22)		
Northeast Point	IHa	Northeast		Andesite
		(1,552±22) Tephra I (1,736±26)		
Southeast Point	GIays	Southeast		Unaltered
Yellow Cliffs	GIays	Southeast		Andesite, extensive alteration
		(1,736±26) Tephra G (3,154±25)		
East Point	Ga	East		Andesite, some alteration

an estimated volume of 0.25 to 0.3 km^3; the missing volume of the edifice, resulting in a horseshoe-shaped crater, is about 0.24 km^3. Siebert and others (1995) suggested that multiple marginal levees and three depositional lobes resulted from an edifice failure which occurred in a retrogressive, closely timed process. The adjacent and underlying Rocky Point debris-avalanche deposit, which is only part exposed, has an estimated volume of 0.15 km^3, including its submarine extent. One of the largest edifice-failure events created the West Island debris-avalanche deposit, which has an approximate volume of 0.5 km^3. Older debris-avalanche deposits elsewhere on the island have patchy subaerial exposure, and most of them have submarine extents; volume estimates for these deposits are unavailable but probably range from 0.25 to 0.5 km^3.

Slope-Stability-Analysis Approach

To assess the future potential slope instability at Augustine Volcano, we use a quasi-3D, "method of columns" limit-equilibrium analysis that quantifies slope stability for different scenarios. Previously, we used this geotechnical approach to analyze the edifice stability at Mount St. Helens and Mount Rainier in Washington State (Reid and others, 2000; Reid and others, 2001) and at Volcán Casita in Nicaragua (Vallance and others, 2004), as well as on coastal bluffs in Seattle, Wash. (Brien and Reid, 2007). Our approach systematically searches the topography as defined by a digital elevation model (DEM) and computes the stability of millions of potential landslides affecting all parts of an edifice; these potential slope failures can encompass a wide range of depths and volumes. After this search is complete, every DEM gridpoint of interest will have been included in some potential landslides. The analysis results in maps portraying the relative stability of all parts of the edifice, the location of the overall least stable potential landslide, and the volumes of potential landslides. Our approach, implemented in the computer program SCOOPS, was detailed by Reid and others (2000) and is briefly described below.

At Augustine Volcano, we are interested in assessing the potential for massive flank collapse in places where the internal structure of the edifice is poorly known. For our analysis, we assumed arcuate potential failure surfaces. Although smaller rock failures are commonly controlled by local discontinuities, such as bedding or jointing surfaces, most large edifice collapses extend deep into the edifice, ignore smaller rock discontinuities, and create arcuate failure surfaces (Siebert, 1984; Voight and Elsworth, 1997). Potential failure surfaces composed of sections of a sphere represent the simplest 3D arcuate geometry unconstrained by internal discontinuities. We did not explicitly analyze the potential effects of internal discontinuities.

Each potential failure mass that we analyzed consists of a group of 3D vertical columns, as defined by the DEM, with a spherical failure surface at depth. Our method, which uses a 3D extension of Bishop's simplified method for two-dimensional rotational failure (Bishop, 1955), can incorporate variable 3D rock properties, 3D pore-fluid-pressure distributions, and simplistic earthquake-shaking effects. The shear resistance of each potential failure mass is given by the

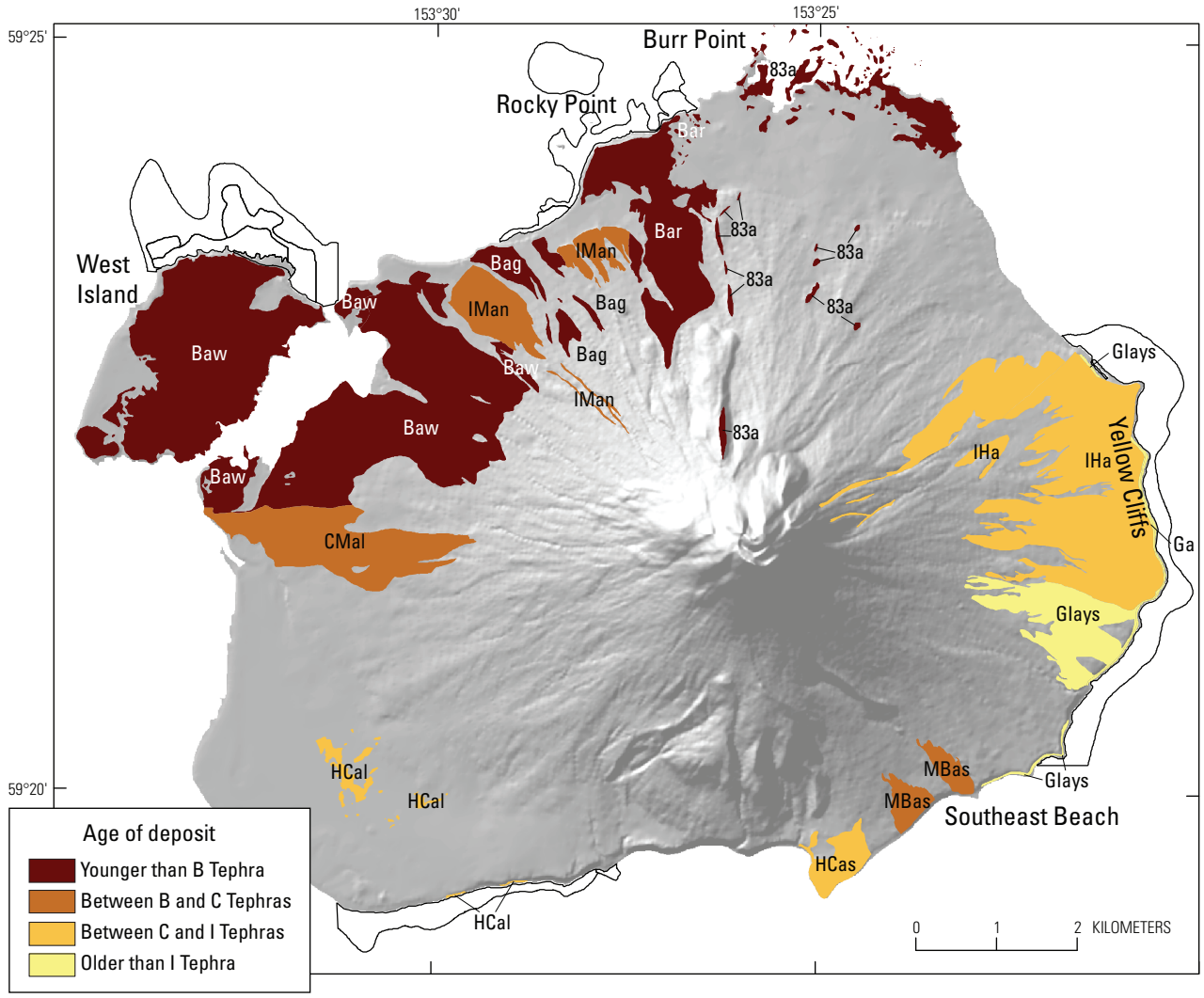

Figure 2. Augustine Island, showing distribution of large debris-avalanche deposits, grouped by age of separating tephra layers. Debris-avalanche unit names and mapped extent from Waitt and Begét (2009). Outlined areas nearshore show extent of some avalanche deposits. Debris-avalanche stratigraphy and tephra ages are listed in table 1. Except for Burr Point, local geographic names (for example, West Island, Rocky Point, Yellow Cliffs, and Southeast Beach) are informal. Shaded-relief image derived from U.S. Geological Survey 10-m digital elevation model (DEM) (unpub. data, 1990).

Coulomb-Terzaghi failure rule, $\tau = c + (\sigma_n - u)\tan\phi$, where c is the cohesion, σ_n is the total normal stress acting on the failure surface (a function of overlying rock weight), u is the pore-fluid pressure on the failure surface, and ϕ is the angle of internal friction. We compute a factor of safety, F, for each potential failure mass, using vertical-force equilibrium and rotational-moment equilibrium, as described by Reid and others (2000). Instability is reflected in F values <1.0; low F values indicate a propensity for collapse. This analysis accounts for the vertical stresses induced by topography and rock weight. We track the minimum F value affecting each DEM point and aggregate the results to produce factor-of-safety maps, as well as associated landslide volumes. If desired, destabilizing earthquake shaking can be incorporated as a pseudostatic horizontal force. Following the approach of Hungr (1987), this force is applied to the base of each vertical column in the potential failure mass (Reid and others, 2000).

Scenarios Analyzed for Augustine Volcano

For our preliminary slope-stability analysis, we need estimates of topography, rock properties (strengths and unit weights), and potential earthquake shaking. A water table at high elevations within the edifice could be destabilizing; such

a condition appeared to facilitate the 1980 collapse of Mount St. Helens (Voight and others, 1983). However, little is known about groundwater conditions at Augustine. Given fractured, permeable rocks in a generic edifice, groundwater-flow modeling suggests that an elevated water table is unlikely (Hurwitz and others, 2003), although localized perched groundwater or fluids in cracks could contribute to future edifice instability. Here, we ignore the possible effects of shallow magma intrusion or elevated pore-fluid pressures. We are interested in larger edifice failures and therefore analyze the stability of potential failures only of volumes from 0.1 to 1.0 km^3.

The pre-2006 topography of Augustine Island is well known, defined by a 10-m DEM derived from a 1:25,000-scale map (U.S. Geological Survey, unpub. data, 1990). A shaded-relief image of this DEM portraying local slope at each DEM node is shown in figure 3. Topographic modifications caused by the 2006 eruption had a relatively minor effect on the overall edifice geometry (fig. 4) and would likely have only minor effects on our analysis. Because we calculate the slope stability of massive failures encompassing large parts of the edifice, we resampled the DEM at a 50-m grid spacing for computational efficiency. For accurate estimates of F value and volume, about 100 DEM columns are needed to define each potential failure mass. Our resampled DEM spacing provides about 400 columns within potential failure masses near the low end of our desired volume range (0.1 km^3). Our search region for slope-stability analysis is limited to steeper sides of the volcanic edifice. Within this search region, we analyze the stability of millions of potential failure masses for each scenario.

A primary control on slope stability is shear strength. Rock properties, such as strength and unit weight, can vary drastically both spatially and temporally within a volcanic edifice. Fresh massive lava flows may be mechanically strong whereas air-fall deposits may be weak; even visually similar rock types may have spatially varying mechanical properties. Progressive acid sulfate-argillic hydrothermal alteration can weaken rocks over time, possibly promoting slope instability (Lopez and Williams, 1993; Watters and others, 2000; Reid and others, 2001).

The upper, steep part of Augustine Volcano is composed primarily of fresh andesite and dacite lava domes (fig. 4) with little or no visible hydrothermal alteration (Waitt and others, 1996; Waitt and Begét, 2009). Visual inspection by the

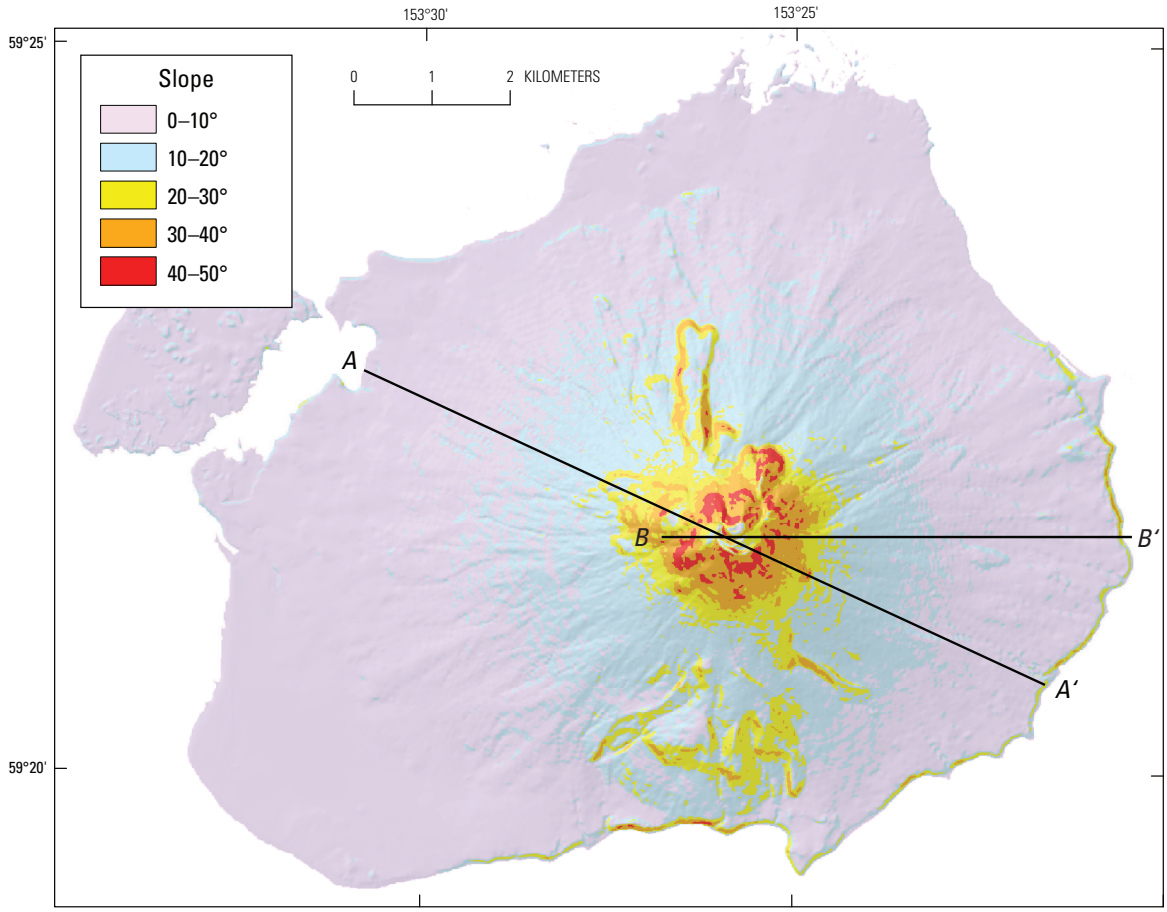

Figure 3. Augustine Island, showing slopes derived from unpublished U.S. Geological Survey (USGS) 10-m digital elevation model (DEM). Steepest slopes occur on upper edifice. Lines *A*–*A*′ and *B*–*B*′, locations of cross sections in figures 4 and 7. Shaded-relief image derived from U.S. Geological Survey 10-m digital elevation model (DEM) (unpub. data, 1990).

first author of the upper domes in 1997 also revealed only localized alteration at fumaroles. Thus, the carapace of the modern Augustine edifice appears to lack widespread acid sulfate alteration. This style of alteration, present at Mount Rainier (Finn and others, 2001), can weaken rocks (Watters and others, 2000) and significantly reduce slope stability (Reid and others, 2001). The upper Augustine edifice, composed primarily of fresh dome rocks, is more nearly uniform than in the notable layering at some other stratovolcanoes. Although nearly all the debris-avalanche deposits derived from the Augustine edifice contain little altered rock, the Yellow Cliffs deposit does contain hydrothermally altered clay. Thus, more altered rocks may be present at depth within the edifice.

For our preliminary slope-stability analysis, we use two end-member scenarios, assuming uniform shear strength (defined by internal angle of friction and cohesion) and unit weight (table 2), representing strong rocks and relatively weak altered rocks. No direct measurements of strength or unit weight are known for Augustine Volcano dome rocks. Cohesion can play a crucial role in defining the volume and depth of a slope failure (Reid and others, 2000), but estimating the cohesion of rocks at depth within an edifice is difficult. Solid, dense igneous rocks can have a cohesion of 10,000 to 100,000 kPa, but highly altered rocks only 10 kPa. Using either surface-rock exposures or debris-avalanche deposits from volcanoes, other researchers have obtained a few measurements of cohesion and internal angle of friction, including at Mount St. Helens (Voight and others, 1983), Mounts Rainier and Hood (Watters and others, 2000), and Citlaltépetl (Zimbelman and others, 2004). We used these published strength values from volcanoes, as well as values determined for other igneous rocks (Jaeger and Cook, 1979; Hoek and Bray, 1981), to constrain our estimates of shear strength. Our end-member scenarios likely bracket values within the Augustine edifice, although Augustine dome rocks probably have properties closer to those of strong rocks (table 2). Rock properties likely vary within the Augustine edifice. Nevertheless, these end members illustrate the possible effects on slope instability.

Finally, we analyzed several scenarios involving large earthquakes. Augustine Island is subject to large tectonic earthquakes with probable ground motions much greater than those of local volcanic or volcano-tectonic origin. Other researchers have estimated probable peak ground accelerations (PGAs) throughout Alaska by combining frequency and magnitude estimates of earthquakes from potential sources with empirical relations for strong-ground-motion attenuation with distance from the source (Wesson and others, 2007). This method estimates strong ground motion for various probabilities of earthquake occurrence. In Alaska, the method takes into account fault sources, such as the Alaska-Aleutian megathrust, and the available seismic record (Wesson and others, 2007). Estimated PGA values are high in much of southern Alaska. From results derived for the Augustine Island region, we selected two PGA values to bracket potential moderate to large earthquakes at Augustine, where a PGA value of 0.35 *g* corresponds to about a 10-percent probability of exceedance in 50 years and a PGA value of 0.5 *g* corresponds to about a 2-percent probability of exceedance in 50 years. As discussed above, these estimated accelerations can be treated as a pseudostatic horizontal force in our analyses. We follow the approach that Voight and others (1983) applied at Mount St. Helens and use the same strength parameters in our ground-shaking scenarios as in our static scenarios. The combination of a static scenario and two ground-shaking scenarios for both strong and weak edifice rocks produces the six scenarios listed in table 2.

Results of Simulations

The minimum stabilities computed by using the program SCOOPS for the six scenarios listed in table 2 are mapped in figure 5, representing the lowest *F* values computed for any potential landslide encompassing each DEM node. Potential landslides with the lowest *F* values are defined as critical failures. The outline of the overall least stable potential landslide (out of about 20 million) computed for each scenario is also shown in figure 5. These results do not necessarily show complete failure masses, except for the overall minimum outlined in black, nor do they indicate that areas with similar *F* values will fail simultaneously. The computed volumes within the target range 0.1 to 1.0 km^3 associated with the least stable

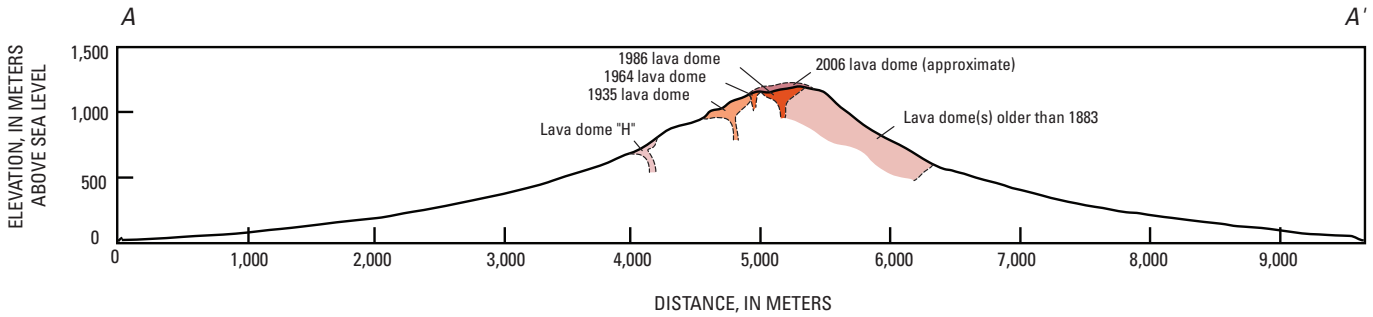

Figure 4. Geologic cross section *A*–*A*′ through Augustine Volcano (see fig. 3 for location), showing dome rocks in upper edifice. Geologic units modified from Waitt and others (1996), with approximate location of 2006 dome added. No vertical exaggeration.

Table 2. Slope-stability scenarios analyzed for Augustine Volcano.

[*F*, factor of safety; PGA, peak ground acceleration]

Scenario	Input				Results	
	Friction angle (°)	Cohesion (kPa)	Unit weight (kN/m³)	Earthquake PGA (*g*)	Minimum *F*	Volume of minimum *F* mass (km³)
1	40	1,000	24	0	2.42	0.13
2	40	1,000	24	0.35	1.35	0.17
3	40	1,000	24	0.5	1.10	0.21
4	28	300	21	0	1.29	0.10
5	28	300	21	0.35	0.71	0.11
6	28	300	21	0.5	0.57	0.11

potential landslide (critical failure) at each DEM node are shown in figure 6. By selecting a point in figure 5, the associated volume can be determined in figure 6.

Variations in potential slope stability induced by differences in rock strength within the Augustine edifice are illustrated in figures 5*A* (uniformly strong rocks) and 5*D* (uniformly weak rocks). These results indicate that (1) a strong-rock edifice has much higher *F* values (min 2.42), whereas a weak-rock edifice has *F* values approaching 1, the limit of stability; (2) the predicted least stable potential landslide is on the upper east flank in both scenarios; and (3) most of the steep upper edifice has *F* values like those of the least stable mass in both scenarios. In these scenarios, potential large landslides have an approximately equal likelihood of initiating from any side of the edifice. Volumes associated with the least stable mass are close to the lower volume limit of 0.1 km³ in both scenarios (figs. 6*A*, 6*D*).

The potentially destabilizing effects of earthquake ground shaking on the Augustine edifice are illustrated in figures 5*B*, 5*C*, 5*E*, and 5*F*. Given a uniformly strong edifice, moderate ground shaking (PGA value, 0.35 *g*) reduces the *F* value throughout the edifice (fig. 5*B*), but the pattern of stability is similar to that of the non-earthquake scenario (fig. 5*A*). In this scenario, the least stable potential landslide (*F* value, 1.35) is still on the east flank, and most of the upper edifice has similar *F* values. Strong ground shaking (PGA value, 0.5 *g*) further reduces the minimum *F* value almost to 1, and the predicted least stable mass is on the east flank. An interesting effect is shown by the increases in volume and depth associated with the least stable potential landslide (fig. 7; table 2): with strong rocks, the least stable volume increases from 0.13 km³ with no shaking, through 0.17 km³ with moderate shaking, to 0.21 km³ with strong shaking.

Given a uniformly weak edifice, *F* values throughout the edifice also decrease with increasing ground shaking (compare figs. 5*D* through 5*F*). As with the strong-rock scenarios, the overall pattern of *F* values remains similar between scenarios. Much of the upper edifice has similar *F* values, and the least stable potential landslide is on the east flank. However, absolute *F* values are considerably lower, and computed minimum *F* values are well below 1 in both the moderate- and strong-ground shaking scenarios (figs. 5*E*, 5*F*; table 2). A pseudostatic-force analysis using peak ground accelerations often produces lower calculated *F* values; therefore, instability can be exaggerated (Seed, 1973; Chowdhury, 1978). In these weak-rock scenarios, all the computed volumes associated with the least stable potential landslides are close to the lower limit of 0.1 km³, suggesting that our preset lower volume limit is controlling the predicted sizes of landslides, rather than are edifice geometry and material properties.

Discussion

The results of our simulations of Augustine edifice stability highlight the effects of topography in controlling the location of potential future slope instability. Large-volume failures integrate destabilizing effects over many DEM nodes. Thus, our maps of calculated slope stability (fig. 5) differ somewhat from a map of local slope at the DEM nodes (fig. 3). Large areas of steep local slope occur on the north and northwest flanks of the edifice (fig. 3), whereas our results indicate that the east flank is potentially the least stable. The relatively small north-northwest-facing theater at the current summit does not appear to exert a strong control on the location of potential large edifice failures. Our results also indicate that most of the steep, upper edifice has similar stabilities for a given scenario, as might be expected for a relatively symmetric cone. This result suggests that in the absence of locally destabilizing events, an approximately equal likelihood exists of a future slope failure affecting any sector of the volcano. Such results agree well with the observation that past debris avalanches have inundated all sectors of the island (Begét and Kienle, 1992; Waitt and Begét, 2009).

Most of the scenarios that we evaluated predict a stable edifice. Parts of the edifice are predicted to become unstable only in scenarios that involve extensive weak, possibly hydrothermally altered rocks and moderate to severe ground shaking. Because Augustine rock strengths are likely nearer those

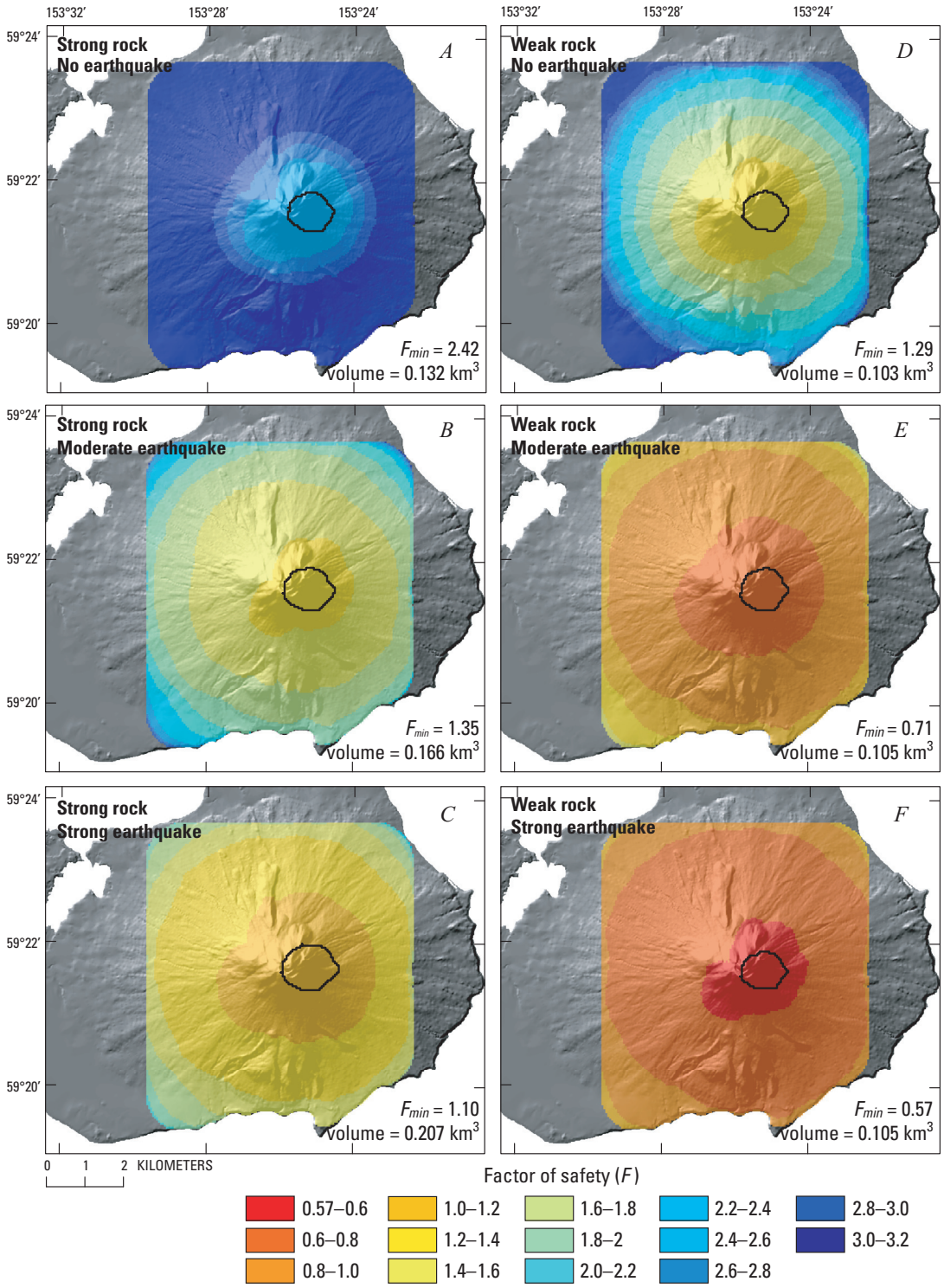

Figure 5. Augustine Volcano, showing computed slope stability of the edifice for six scenarios listed in table 2. Lowest computed factor of safety (*F*) for any potential landslide intersecting each digital elevation model (DEM) node (critical failure) is shown for area searched in our analysis. Warmer colors indicate lower stability; orange and red areas are potentially unstable. Black outline, area of predicted overall least stable potential landslide; minimum factor of safety (F_{min}) and volume associated with this potential landslide are denoted on each diagram. *A*, Scenario 1, with strong rock and no earthquake ground shaking. *B*, Scenario 2, with strong rock and moderate earthquake ground shaking. *C*, Scenario 3, with strong rock and strong earthquake ground shaking. *D*, Scenario 4, with weak rock and no earthquake ground shaking. *E*, Scenario 5, with weak rock and moderate earthquake ground shaking. *F*, Scenario 6, with weak rock and strong earthquake ground shaking. Shaded-relief image derived from U.S. Geological Survey 10-m digital elevation model (DEM) (unpub. data, 1990).

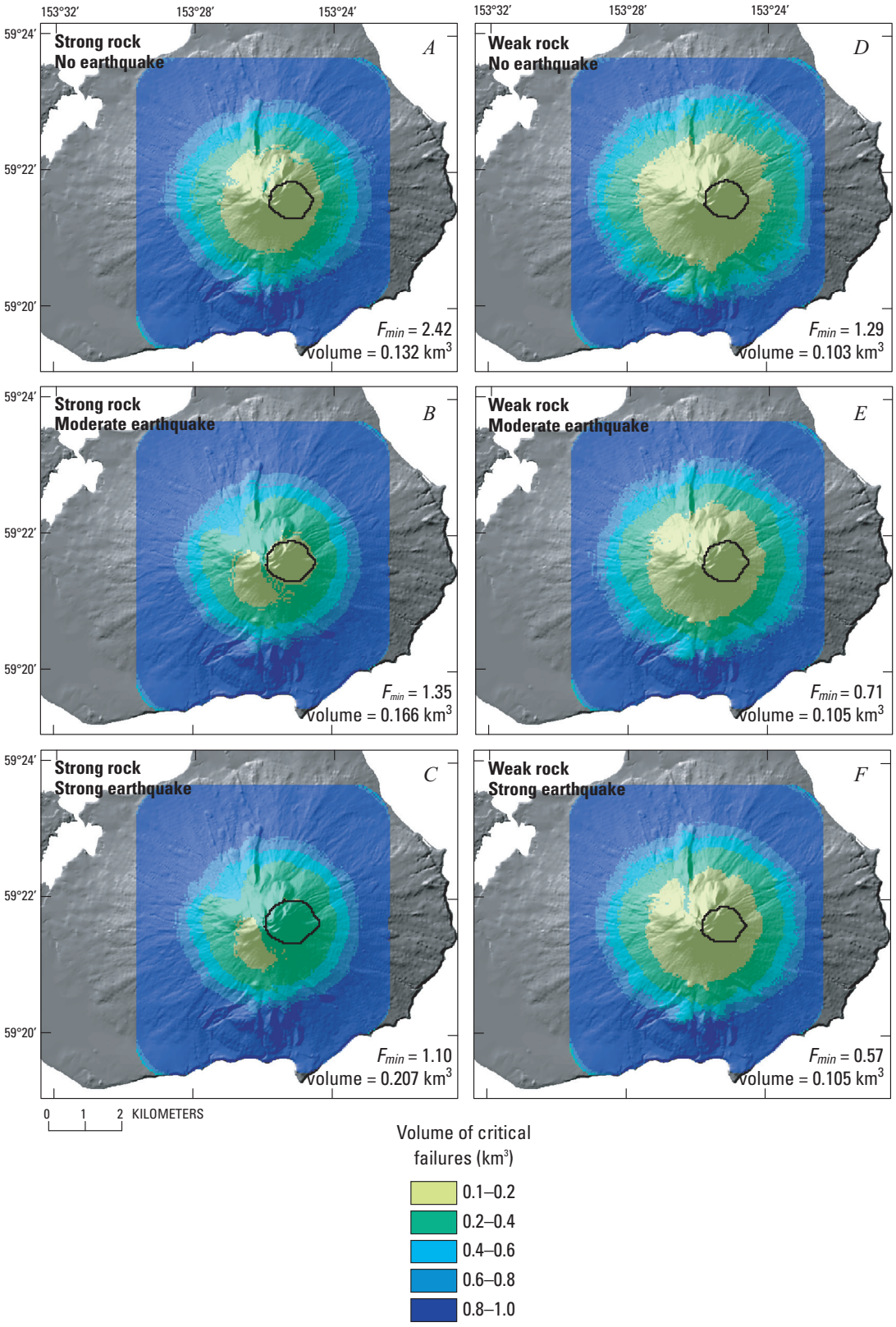

Figure 6. Augustine Volcano, showing potential landslide volumes associated with computed stability of critical failures shown in figure 5. Black outline, area of predicted least stable potential landslide. Six scenarios (*A*-*F*) shown are summarized in figure 5 and listed in table 2. Shaded-relief image derived from U.S. Geological Survey 10-m digital elevation model (DEM) (unpub. data, 1990). See figure 5 for explanation of abbreviations.

of strong rocks, our results suggest that the edifice is unlikely to undergo a massive landslide triggered solely by gravitational failure or a moderate earthquake. Even in scenarios with pervasive weak rocks, slopes are unlikely to fail by gravity alone (fig. 5*D*), implying that additional triggering mechanisms, such as shallow magma intrusion, local oversteepening caused by deformation, and (or) thermal pressurization of pore fluids or gases, are needed to provoke massive collapse at Augustine Volcano.

Although predicted least stable landslide volumes in most of our scenarios are near the lower limit of 0.1 km^3, this analysis does not directly account for retrogressive failure, as occurred at Mount St. Helens in 1980 (Voight and others, 1983; Voight and Elsworth, 1997). At Mount St. Helens, a retrogressive style of collapse increased the failure volume from about 0.8 km^3 for the initial slide block to 2.3 km^3 for all three slide blocks (Voight and others, 1983; Reid and others, 2000). In addition, failed rock masses typically expand as they move downslope. At Mount St. Helens, the volume increased from 2.3 km^3 of source rock to about 2.8 km^3 of debris-avalanche deposit (Voight and others, 1983). At Augustine, both failure retrogression and dilation of debris could enlarge a debris avalanche from its initial failure volume. Stress changes in the subsurface induced by shallow magma intrusion or thermal pressurization could also instigate a larger initial landslide.

A future edifice collapse that produces a debris avalanche with a volume >0.1 km^3 would likely reach the ocean and could generate a tsunami. Our preliminary results suggest that the likelihood of collapse is nearly equal on all sides of the island, although the travel distance from source to coast varies around the island. However, our results indicate that the east flank is marginally less stable. Any avalanche from this flank would travel into deep water, which can enhance the formation of larger tsunamis (Waythomas and others, 2006). A tsunami generated on this side of the island would be directed more toward the southwestern part of the Kenai Peninsula (fig. 1) and the town of Homer (~110 km away) than would a tsunami initiated on the north (as in 1883) or west side of the island.

This preliminary slope-stability analysis focuses primarily on the effects of topography and earthquake shaking. It does not account for spatially varying rock properties within the edifice, the occurrence of such dynamic triggers as shallow magma intrusion or thermal pressurization, or potential retrogression of an initial failure into the edifice. Also, we did not evaluate possible changes in slope stability induced by new lava-dome growth during the 2006 eruption. Nevertheless, our results highlight potential failure locations, given reasonable assumptions about the Augustine edifice. With additional research, rock properties might be better defined, although determining them for rocks at potential failure depth deep within the edifice would be difficult. Possible dynamic triggering events might also be better modeled. Future instability at Augustine Volcano will likely be accompanied by volcanic unrest. Monitoring seismicity and ground deformation should aid in detecting shallow magma movement and may help in short-term forecasting of impending edifice failure.

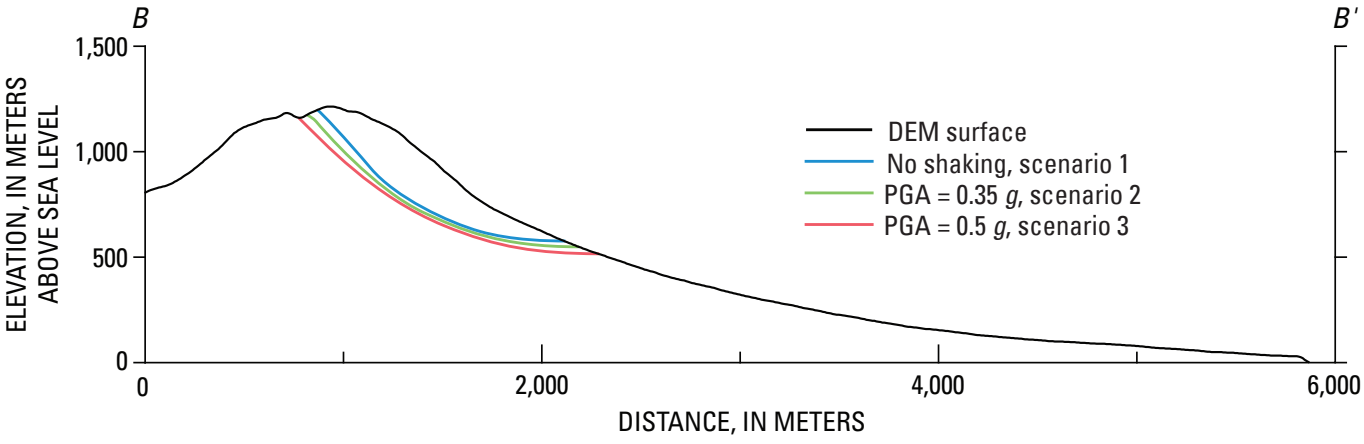

Figure 7. Cross section *B–B′* through Augustine Volcano (see figure 3 for location), showing predicted least stable potential landslide surfaces for scenarios 1 (no earthquake shaking), 2 (moderate ground shaking with peak ground acceleration = 0.35 *g*), and 3 (strong ground shaking with peak ground acceleration = 0.5 *g*), all with strong rocks. Volume of predicted least stable landslide increases with increasing strength of ground shaking (table 2). No vertical exaggeration. DEM, digital elevation model; PGA, peak ground acceleration.

References Cited

Begét, J.E., Gardner, C., and Davis, K., 2008, Volcanic tsunamis and prehistoric cultural transitions in Cook Inlet, Alaska: Journal of Volcanology and Geothermal Research, v. 176, p. 377–386.

Begét, J.E., and Kienle, J., 1992, Cyclic formation of debris avalanches at Mount St. Augustine volcano: Nature, v. 356, no. 6371, p. 701–704.

Begét, J.E., and Kowalik, Z., 2006, Confirmation and calibration of computer modeling of tsunamis produced by Augustine Volcano, Alaska: Science of Tsunami Hazards, v. 24, no. 4, p. 257–266.

Bishop, A.W., 1955, The use of slip circles in the stability analysis of slopes: Geotechnique, v. 5, p. 7–17.

Brien, D.L., and Reid, M.E., 2007, Modeling 3-D slope stability of coastal bluffs using 3-D ground-water flow, southwestern Seattle, Washington: U.S. Geological Survey Scientific Investigations Report 2007-5092, 54 p. [http://pubs.usgs.gov/sir/2007/5092/].

Chowdhury, R.N., 1978, Slope analysis: Amsterdam, Elsevier, v. 22, 423 p.

Davidson, G., 1884, Notes on the volcanic eruption of Mount Saint Augustine, Alaska, October 6, 1883: Science, v. 3, no. 54, p. 186–189.

Finn, C.A., Sisson, T.W., and Deszcz-Pan, M., 2001, Aerogeophysical measurements of collapse-prone hydrothermally altered zones at Mount Rainier volcano: Nature, v. 409, p. 600–603.

Glicken, H., 1991, Sedimentary architecture of large volcanic-debris avalanches, *in* Fisher, R.V., and Smith, G.A., eds., Sedimentation in volcanic settings: Santa Barbara, Calif., Society of Economic Paleontologists and Mineralogists, p. 99–106.

Hoek, E., and Bray, J.W., 1981, Rock slope engineering (3d ed.): London, Institute of Mining and Metallurgy, 358 p.

Hungr, O., 1987, An extension of Bishop's simplified method of slope stability analysis to three dimensions: Geotechnique, v. 37, no. 1, p. 113–117.

Hurwitz, S., Kipp, K.L., Ingebritsen, S.E., and Reid, M.E., 2003, Groundwater flow, heat transport, and water table position within volcanic edifices—Implications for volcanic processes in the Cascade Range: Journal of Geophysical Research, v. 108, no. B12, DOI: 10.1029/2003JB002565.

Jaeger, J.C., and Cook, N.G.W., 1979, Fundamentals of rock mechanics (3d ed.): New York, Chapman and Hall, 593 p.

Kienle, J., Kowalik, Z., and Murty, T.S., 1987, Tsunamis generated by eruptions from Mount St. Augustine volcano, Alaska: Science, v. 236, no. 4807, p. 1442–1447.

Kienle, J., and Swanson, S.E., 1985, Volcanic hazards from future eruptions of Augustine Volcano, Alaska (2d ed.): Fairbanks, University of Alaska, Geophysical Institute Report UAG-R 275, 122 p.

Lander, J.F., 1996, Tsunamis affecting Alaska: Boulder, Colo., U.S. National Oceanic and Atmospheric Administration, National Environmental Satellite Data and Information Service, National Geophysical Data Center, 195 p.

Lopez, D.L., and Williams, S.N., 1993, Catastrophic volcanic collapse; relation to hydrothermal processes: Science, v. 260, no. 5115, p. 1794–1796.

Miller, T.P., McGimsey, R.G., Richter, D.H., Riehle, J.R., Nye, C.J., Yount, M.E., and Dumoulin, J.A., 1998, Catalog of the historically active volcanoes of Alaska: U.S. Geological Survey Open-File Report 98-0582, p. 104.

Reid, M.E., 2004, Massive collapse of volcano edifices triggered by hydrothermal pressurization: Geology, v. 32, no. 5, p. 373–376.

Reid, M.E., Christian, S.B., and Brien, D.L., 2000, Gravitational stability of three-dimensional stratovolcano edifices: Journal of Geophysical Research, v. 105, no. B3, p. 6043–6056.

Reid, M.E., Sisson, T.W., and Brien, D.L., 2001, Volcano collapse promoted by hydrothermal alteration and edifice shape, Mount Rainier, Washington: Geology, v. 29, no. 9, p. 779–782.

Seed, H.B., 1973, Stability of earth and rockfill dams during earthquakes, *in* Hirshfeld, R.C., and Poulos, S.J., eds., Embankment-dam engineering: New York, Wiley and Sons, p. 239–269.

Siebert, L., 1984, Large volcanic debris avalanches; characteristics of source areas, deposits, and associated eruptions: Journal of Volcanology and Geothermal Research, v. 22, p. 163–197.

Siebert, L., and Begét, J.E., 2006, Two millennia of edifice instability at Augustine Volcano, Alaska and implications for future collapse: Eos, American Geophysical Union Transactions, v. 87, no. 52, fall meeting supp., abstract V51C-1692.

Siebert, L., Begét, J.E., and Glicken, H., 1995, The 1883 and late-prehistoric eruptions of Augustine volcano, Alaska: Journal of Volcanology and Geothermal Research, v. 66, p. 367–395.

Siebert, L., Glicken, H., and Kienle, J., 1989, Debris avalanches and lateral blasts at Mount St. Augustine volcano, Alaska: National Geographic Research, v. 5, no. 2, p. 232–249.